Douwe S. de Bruijn

Master Thesis

Electrowetting-Controlled Diode-Like Behavior of Suspended Graphene Membranes

---

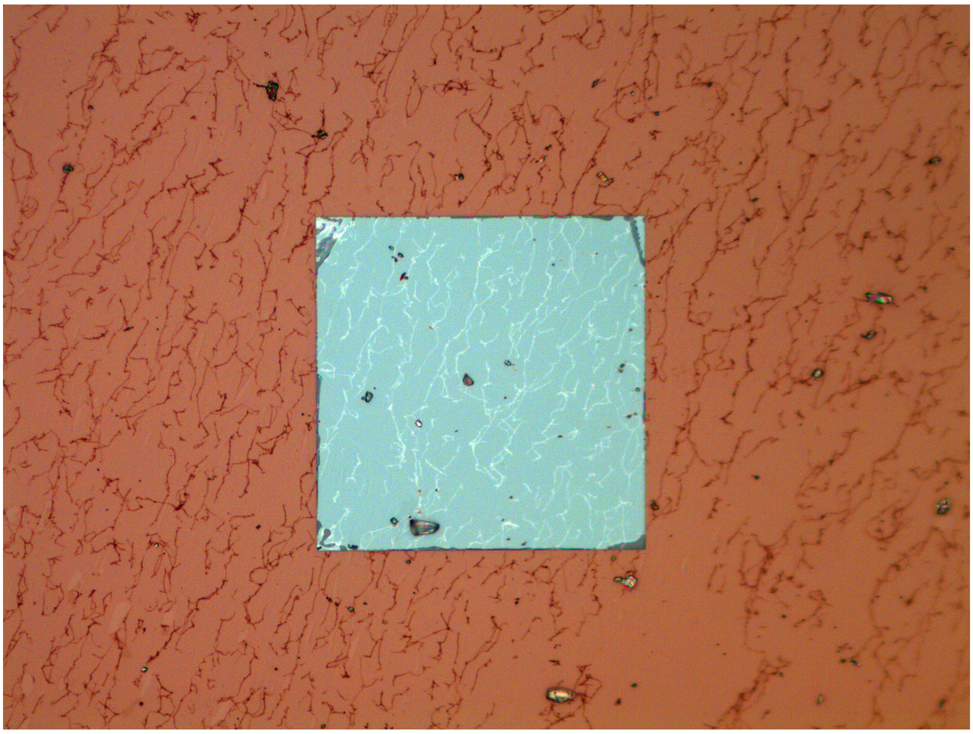

BIOS Lab-on-a-Chip Group
Electrical Engineering
University of Twente

April 2018

UNIVERSITY OF TWENTE.

Faculty of Electrical Engineering,
Mathematics & Computer Science

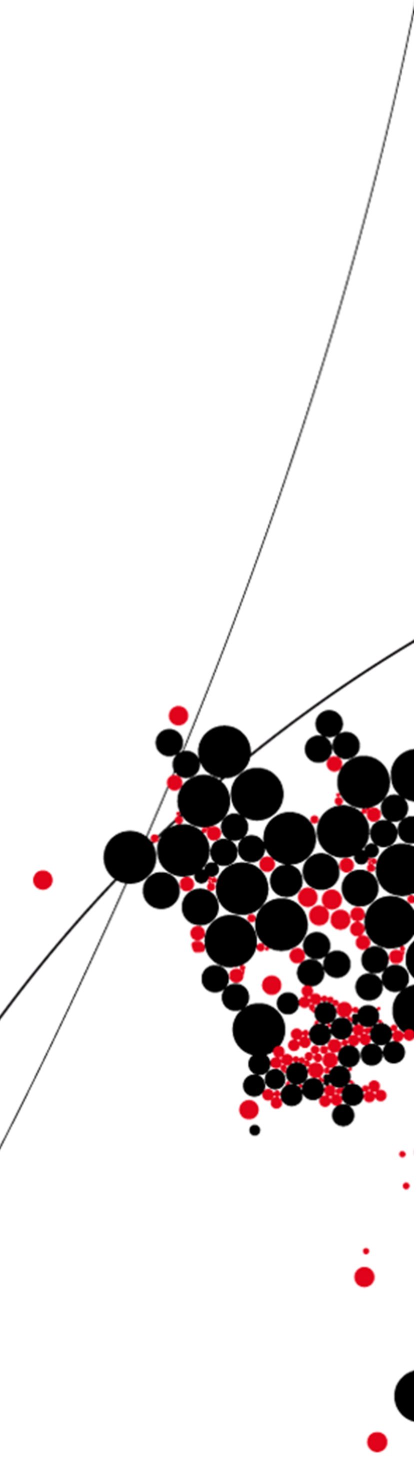

Electrowetting-Controlled Diode-Like Behavior of Suspended Graphene Membranes

Douwe S. de Bruijn
M.Sc. Thesis
April 2018

Supervisors
Prof. dr. Jan Eijkel
Joshua Loessberg-Zahl, M.Sc.
Vasileios Papadimitriou, M.Sc.
Examining committee
Prof. dr. Jan Eijkel
Joshua Loessberg-Zahl, M.Sc.
Vasileios Papadimitriou, M.Sc.
Dr. Ir. Wesley van den Beld
Prof. Dr. Ir. Harold Zandvliet
Dr. Ir. Wouter Olthuis

BIOS Lab-on-a-Chip Group
University of Twente

Contents

Chapter 1

Introduction

In this research the electrowetting of suspended graphene membranes on a silicon nitride (SiN) substrate has been studied and observed. In addition, a resistor based model is supported by measurements of the voltage dependent conductance of the system. The system of interests is shown in figure 1.1. The suspended graphene is nanoporous and allows for charge transport when a potential over the membrane is applied. At a certain threshold voltage the graphene starts to detach from the SiN substrate and an increase in conductance is observed, as is show in figure 1.2. This diode-like current voltage behavior has first been observed by Wesley van den Beld and Joshua Loessberg-Zahl[1].

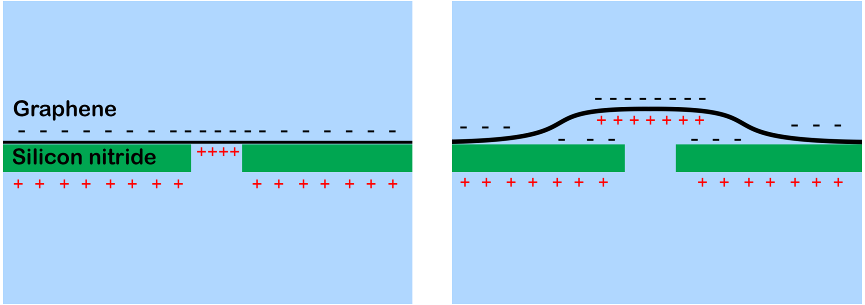

FIGURE 1.1: Schematic overview of the system. The graphene is indicated in black and the SiN in green. A potential is applied across the membrane, resulting in a charge distribution denoted by + and -. The blue indicates a 1 M KCl electrolyte to which the potential is applied and the top and bottom reservoir are electrically isolated. In the left figure the graphene is still attached to the SiN membrane. The right figure shows detachment of the graphene from the SiN membrane at higher voltage. We predict that this is caused by electrowetting. The detached graphene allows for more ion transport through newly exposed graphene nanopores, resulting in an increased current.

A lot of research is done on these ultra-thin nanopore devices[2]–[4], which are theoretically valuable for application fields like DNA sequencing[2] and desalination[5]. Graphene has perfect properties for these application areas, because it is ultra thin[6], has mechanical strength[7] and has appropriate pores, which enable size selective filtration[8], [9]. However, in literature voltages above 0.2 V are normally avoided, because the increased conductivity at higher voltage is not well understood in the existing literature that we found [3], [4], [10].

The goal of this master thesis is to confirm that electrowetting occurs and get a better understanding of the processes playing a role in the system. Three different experimental techniques have been used to get deeper insight in the system. Firstly, electrochemical measurements have been conducted to expand the current dataset.

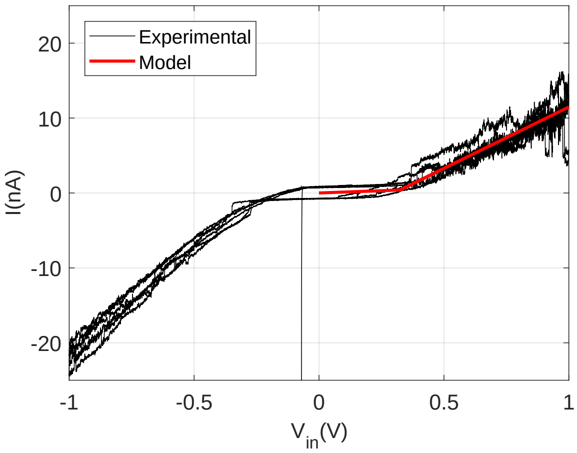

FIGURE 1.2: Typical cyclic voltammetry (CV) experiment (black) and the modeling results (red).

Secondly, optical images have been recorded during the electrochemical measurements to observe changes in the SiN-graphene interface. Lastly, the height profile of the graphene has been measured while different constant potentials were applied using atomic force microscopy (AFM).

The combined results of the described measuring techniques have shown the detachment of the graphene from the SiN substrate. Furthermore, the output of the resistor model matches the experimental data without fitting and has clearly demonstrated the voltage dependent detachment of the graphene from the substrate. The presented results show new insight in the processes at play, which might help future research to control and mitigate the detachment of the graphene from the SiN substrate.

Chapter 2

Theory

Different phenomena play a role at the SiN-graphene interface. The diversity of the potential distributions, charge distributions and chemical surfaces processes creates a very rich system. The surface phenomena will first be discussed. These phenomena facilitate the attachment and detachment of the graphene to the SiN substrate. Next, a few graphene properties are highlighted. Subsequently, several transport phenomena in the SiN-electrolyte-graphene system are explored. The charge transport in the system is then simplified by modeling the system as a resistor network. Finally, basic electrochemistry is explained.

2.1 Surface interactions and phenomena

Four phenomena at the SiN-graphene interface are discussed: Van der Waals forces, the electrical double layer, the interfacial capacitance and electrowetting. The surface interaction between the SiN-graphene interface are created by Van der Waals forces and the electrical double layer (EDL). Van der Waals forces provide an attractive force between the graphene and SiN interface, creating an associated adhesion energy. When a potential is applied to the system, the EDL is charged like a capacitor giving it a competing surface energy. At some point the energy of the capacitor overcomes the Van der Waals forces and it becomes energetically preferable for the capacitor to spread, thus the graphene detaches. The detachment, due to the applied potential is better known as electrowetting. The interplay of the Van der Waals forces, EDL and interfacial capacitance govern the dynamics of the electrowetting in our system.

2.1.1 Electrical double layer and Van der Waal forces

An (electrical) double layer (EDL) can be formed at a solid liquid interface. It is a physical phenomena describing the accumulation of counter-ions in the fluid close to surface. The ions are attracted by a surface charge, which can be induced by chemical interactions and/or an external electric field. The surface charge is screened over a particular length by all the ions. The screening length is better known as the Debye length κ^{-1} and is a function of the salt concentration c in the electrolyte. The more ions available, the easier the screening and the shorter the Deybe length. An approximation of the Debye length for symmetric monovalent electrolytes is given by equation 2.1 [11].

$$\kappa^{-1} = \sqrt{\frac{\epsilon\epsilon_0 RT}{2F^2 c}} \tag{2.1}$$

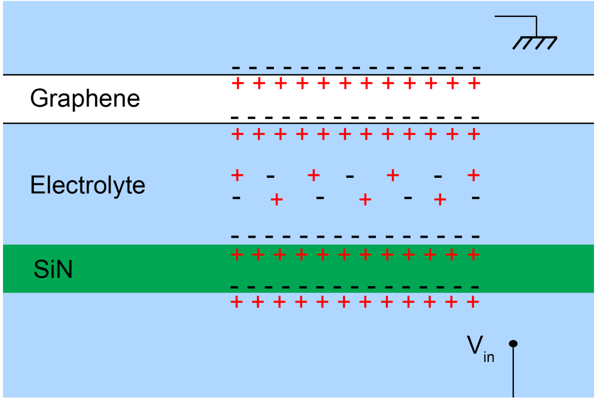

FIGURE 2.1: Schematic of all charges in the system. An EDL is formed close the surface of the SiN and graphene. In this representation there is no EDL overlap, meaning that all surface charges are screened by counter-ions. This results in zero net charge in the middle of the channel.

with ϵ the dielectric constant, ϵ_0 the absolute permittivity, R the gas constant, T the temperature, F Faraday's constant and c the bulk concentration. For a 1 M KCl electrolyte at room temperature the Debye length κ^{-1} is $\kappa^{-1} \approx 0.3\,\text{nm}$.

In case of the electrolyte-graphene interface the surface is screened by positive or negative ions depending on the polarization of the applid potential. In the schematic of figure 2.1 the graphene's surface is negatively charged at the SiN side, therefore positive ions are attracted from the electrolyte in the channel. As a result the accumulated charge at the interface forms a conduction path.

Once all the surface charges are screened by counter-ions the net charge in the fluid is zero as can be seen in the middle of the channel in figure 2.1. In this case electrostatics play no role. However, there is an attractive electrostatic force when the EDLs overlap each other. This occurs when the Deybe length increases due to a lower salt concentrations or when the interfaces are more close together. In case two opposing interfaces have the same surface charge, the EDL force is repulsive. In both cases the EDL force falls off over distance x with $E_{\text{EDL}}(x) \propto \kappa^{-1} e^{-x\kappa^{-1}}$.

The Van der Waals forces are distance-dependent interactions between atoms and molecules. These forces describe multiple intermolecular forces, which can be attractive and repulsive. In case of a graphene-SiN interface the forces are attractive, but vanishes quickly over distance x with $E_{\text{vdw}}(x) \propto -x^{-2}$ and $\sim z^{-3}$[12]. The Van der Waals forces are the dominating forces at close distance, which keep the graphene-SiN interface closely attached together. The energy needed to separate the graphene from the SiN substrate is called the adhesion energy. The adhesion of the two interfaces can be improved by decreasing the substrate roughness and minimalizing contamination on the substrate[13]. The respulsive EDL force will drive the two interfaces apart, which is explained in the secion 2.1.3.

2.1.2 Interfacial capacitance

In the system two different interfaces can be found. One electrolyte-graphene interface and an electrolyte-SiN interface as illustrated in figure 2.2. The interfacial capacitance C_{int} is the product of multiple capacitances in series as described by equation 2.2[14].

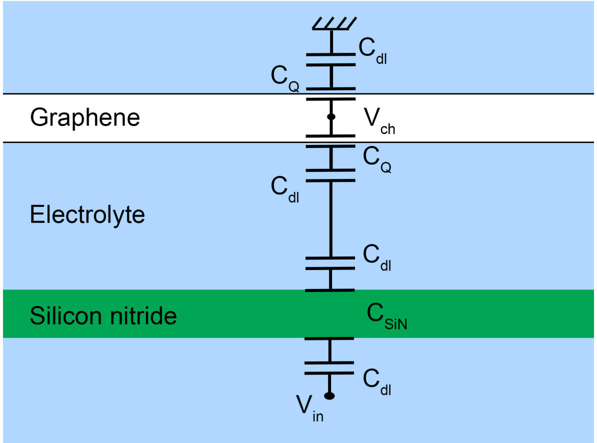

FIGURE 2.2: Schematic representation of the capacitances in the system. At all the surface-electrolyte interface EDLs (C_{dl}) are formed. Furthermore, the quantum capacitance of the graphene (C_{Q}) and the charge induced capacitance over the SiN membrane (C_{SiN}) are indicated.

$$C_{\mathrm{int}} = \frac{1}{C_{\mathrm{Q}}} + \frac{1}{C_{\mathrm{diff}}} + \frac{1}{C_{\mathrm{H}}} \tag{2.2}$$

The first term in the equation accounts either for the space charge capacity in a semiconductor interface or the quantum capacitance C_{Q} at a graphene interface[14], [15]. The last two terms are the diffuse double layer C_{diff} and the Helmholtz double layer C_{H}, which represent the capacitance of the electrical double layer (EDL) C_{dl}. In concentrated electrolytes, $C_{\mathrm{diff}} \gg C_{\mathrm{H}}$ and therefore C_{diff} can be neglected[14]. For monolayer graphene in 1 M KCl the double layer capacitance C_{dl} is approximately $\sim 0.2\,\mathrm{Fm}^{-2}$[16].

Graphene has special electrostatic properties such as its quantum capacitance C_{Q}, due to a lack of electron density of states[17]. Research has shown that the quantum capacitance plays a significant role in the interfacial capacitance of single layer grapehene, because it is much smaller than the double layer capacitance[15], [18]. The specific quantum capacitance is defined in equation 2.3[17] and depends on the local potential of graphene V_{ch}. However, in previous research the graphene layer is always gated, such that V_{ch} is actively controlled[15], [18]–[20]. In the described system the graphene is floating and not gated. No research has been found describing the capacitive behavior of an electrically floating sheet of graphene. Two different situations will be considered to model the interfacial capacitance of the graphene. The first situation simply assumes a double plate capacitor C_{p} with a dielectric constant $\epsilon_{\perp} =\sim 3.5$[21], graphene monolayer thickness $t = 0.37\,\mathrm{nm}$[6] and no quantum capacitance, resulting in $C_{\mathrm{p}} = \epsilon_{\perp}\epsilon_0/t = 0.08\,\mathrm{Fm}^{-2}$. In this case the graphene capacitance is not dependent on the voltage and dominates the interfacial capacitance of the graphene ($C_{\mathrm{dl}} \gg C_{\mathrm{p}}$).

The second situation considers that the floating potential in the graphene contributes to a quantum capacitance. The potential on the graphene is assumed to be the average of the potential on either side. This potential follows from the symmetry in the electrolyte-graphene-electrolyte interface as can be seen in figure 2.2. In that case V_{ch} equals half the local potential across the graphene V_{gr}.

$$C_{\mathrm{Q}} = \frac{2e^2 k_{\mathrm{B}} T}{\pi(\hbar v_{\mathrm{f}})^2} \ln\left[2\left(1 + \cosh(\frac{eV_{\mathrm{ch}}}{k_{\mathrm{B}} T})\right)\right] \tag{2.3}$$

with e the elementary charge, k_{B} the Boltzmann constant, $\hbar$ the Planck constant and v_{f} the Fermi velocity of the Dirac electron. At room temperature this equation can be linearized, because $eV_{\mathrm{ch}} \gg k_{\mathrm{B}} T$ for tens of millivolts, resulting in equation 2.4[17].

$$C_{\mathrm{Qlin}} = \alpha V_{\mathrm{ch}} \quad \text{where} \quad \alpha = \frac{2e^3}{\pi(\hbar v_{\mathrm{f}})^2} \tag{2.4}$$

A comparison between the quantum capacitance including the double layer capacitance and the plate capacitor approach is shown in figure 2.3. The quantum capacitance curve shows the expected voltage dependent symmetric V-shape [20]. The double plate capacitor approach and the interfacial capacitance are in the same order of magnitude between 0.3 V and 1 V. Only at very low potential do the two approaches deviate dramatically.

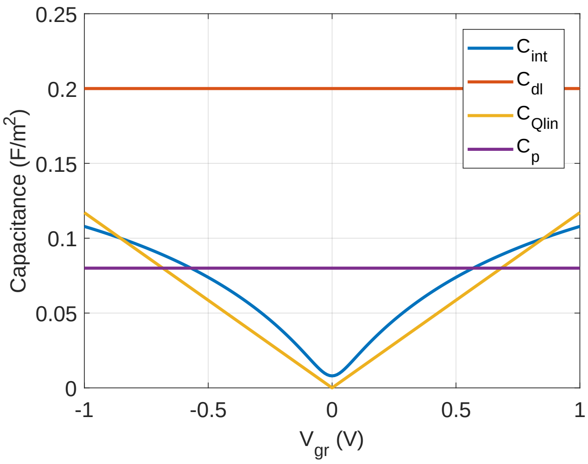

FIGURE 2.3: Comparison of the interfacial capacitance C_{int} ($C_{\mathrm{dl}} + C_{\mathrm{Qlin}}$), the double layer capacitance C_{dl}, the linear quantum capacitance C_{Qlin} and the plate capacitor model C_{p} versus the applied potential across the graphene.

The found values for the interfacial capacitance of graphene are put into perspective by expressing the SiN interfacial capacitance. Due to a lack of literature on the surface chemistry of SiN, the better known silicon dioxide(SiO_2) interface is considered to give expression to the specific EDL capacitance of the SiN membrane. This is a fair assumption, since the SiN substrate in the used device is strongly oxidized, creating silanol groups. The specific EDL capacitance of SiO_2 is reported as $0.8\,\mathrm{Fm^{-2}}$[22]. However, the charge induced capacitance of the 40 nm thick SiN membrane is in this case much more dominant for the interfacial capacitance of the SiN: $C_{\mathrm{SiN}} = \epsilon\epsilon_0/t = 0.002\,\mathrm{Fm^{-2}}$ with $\epsilon = 8$.

The interfacial capacitance of the graphene is, in both considered cases, approximately factor 40 bigger than the interfacial capacitance of SiN. Therefore, the interfacial capacitance of graphene dominates the charged-based behavior at the SiN-graphene interface.

2.1.3 Electrowetting

Electrowetting is the effect of a change in contact angle of a solid-electrolyte interface when an electric field is applied over the interface[23]. A force due to the applied electric field is created by induced charge at the EDL, which creates an osmotic (disjoint) pressure. For electrowetting to happen in the system $E_{\text{cap}} > \Delta\gamma_{\text{adh}}$, where E_{cap} is the energy of the charged interfacial capacitance and $\Delta\gamma_{\text{adh}}$ the interfacial energy between the graphene and the SiN substrate as a result of the Van der Waals forces. The capacitive energy is the result of the charged interfacial capacitance as is expressed in equation 2.5[23], [24]. This equation assumes an uniform surface and the voltage drop over the interface. From this equation follows that a certain threshold voltage must be overcome in order for electrowetting to happen.

$$\frac{1}{2} C_{\text{int}} V^2 > \Delta\gamma_{\text{adh}} \tag{2.5}$$

The net interfacial energy $\Delta\gamma_{\text{adh}}$ follows from the interfacial energy between the graphene and the substrate $\gamma_{\text{Gr}-\text{SiO}_2}$ minus the interfacial energy between the graphene and the electrolyte $\gamma_{\text{SiO}_2-\text{H}_2\text{O}}$ and the substrate and the electrolyte $\gamma_{\text{Gr}-\text{H}_2\text{O}}$, as is shown in equation 2.6. Due to strong oxidation of the surface, the better known SiO_2 substrate is again considered.

$$\Delta\gamma_{\text{adh}} > \gamma_{\text{Gr}-\text{SiO}_2} - \gamma_{\text{SiO}_2-\text{H}_2\text{O}} - \gamma_{\text{Gr}-\text{H}_2\text{O}} \tag{2.6}$$

The interfacial adhesion between the graphene and the SiO_2 substrate is strongly dependent on the surface structure of the substrate and the number of water layers[25]. The upper limit of the net interfacial energy is determined, such that a maximum threshold voltage $V_{\text{T,max}}$ for electrowetting can be expressed. The upper limit of $\gamma_{\text{Gr}-\text{SiO}_2}$ is estimated at $\sim 0.45\,\text{Jm}^{-2}$ for monolayer graphene with no water layers between the two surfaces[26]. The other two interfacial energies are $\gamma_{\text{SiO}_2-\text{H}_2\text{O}} = 0.26\,\text{Jm}^{-2}$[27] and $\gamma_{\text{Gr}-\text{H}_2\text{O}} = 0.029\,\text{Jm}^{-2}$[28]. An upper limit of $\Delta\gamma = 0.16\,\text{Jm}^{-2}$ follows from the given parameters. Subsequently, the maximum threshold voltage $V_{\text{T,max}} = 1.0\,\text{V}$ follows from our previous estimation of the interfacial capacitance of graphene as $C_{\text{p}} = 0.08\,\text{Fm}^{-2}$. This is purely an estimate and large variations from system to system are expected, because the graphene is not perfect and the SiN substrates will not be perfectly smooth. Furthermore, as a result of the decaying EDL force, as explained in section 2.1.1, the height of the detached graphene is expected to be a couple of κ^{-1}.

2.2 Graphene defects and optical properties

In this research defects in the graphene are exploited as nanopores. The types, sizes and density of defects are discussed. Furthermore, graphene has particular optical behavior, which will be used to characterize the number of graphene layers.

2.2.1 Defects

Graphene is grown on copper using chemical vapor deposition (CVD) as explained in section 3.1.1. The advantage of this method is the natural occurrence of intrinsic defects, which saves the process of generating nanopores in defect-less exfoliated graphene. CVD graphene is polycrystalline contrary to pristine graphene, which result in imperfections at the grain boundaries. The copper is exposed to methane and acts as a catalyst to dissociate the methane, which starts the nucleation of graphene islands at multiple positions. At some point the domains meet and coalesce to form a continuous layer.

Several types of defects can be distinguished: dislocation in the crystal (known as Stone-Wales defect), point defects in the graphene and stitching defects at grain boundaries[1]. The point defects, as shown in figure 2.4, are the defects of interest. Literature reports that these defects can be the result of impurities on the copper surface and have an estimated spacing of 70 nm to 100 nm and the majority of the defects have a defect size that ranges from 0.5 nm to 2 nm [29], [30].

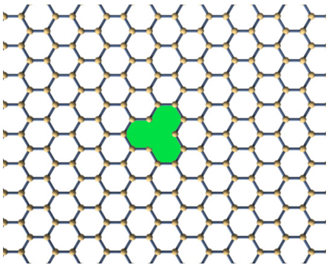

FIGURE 2.4: Point defect in the graphene structure as a result of impurities on the copper surface.

2.2.2 Optical

Raman spectroscopy can be used to determine the number of graphene layers and the quality of the graphene. This technique makes use of a rare physical event: inelastic scattering of photons. When light of a certain wavelength interacts with matter most photons are scattered with the same energy as the incident photons. This is known as elastic scattering. However, a rare fraction of the photons are involved in an inelastic scattering event, which results in a different (usually lower) energy of the scattered photons. The change in energy of the scattered photons, due to inelastic scattering is called the Raman effect. The energy shift gives crucial information about molecular vibration, which is a fingerprint for the type and coordination of molecules involved in the scattering process.

A Raman spectrum shows the intensity of scattered light versus the wavenumber in cm^{-1} and is centered around the wavelength of the incident light, known as the Rayleigh line (defined as $0\,\mathrm{cm}^{-1}$). Several peaks that are typical for graphene on a SiO_2 substrate can be identified in the Raman spectrum as schematically shown in figure 2.5. The peaks of interest are called the D, G and $2D$ peak. Their shape, width and position gives information about the graphene. The width of the peaks is expressed as the full width at half maximum (FWHM). A sharp $2D$ peak at $\sim 2700\,\mathrm{cm}^{-1}$, which is more intense than the G peak at $\sim 1580\,\mathrm{cm}^{-1}$, suggests monolayer graphene. Likewise a slight downshift of the G peak position indicates for an increase in graphene layers [31], [32]. The D peak at $\sim 1350\,\mathrm{cm}^{-1}$ is a measure for the number of defects[32], [33].

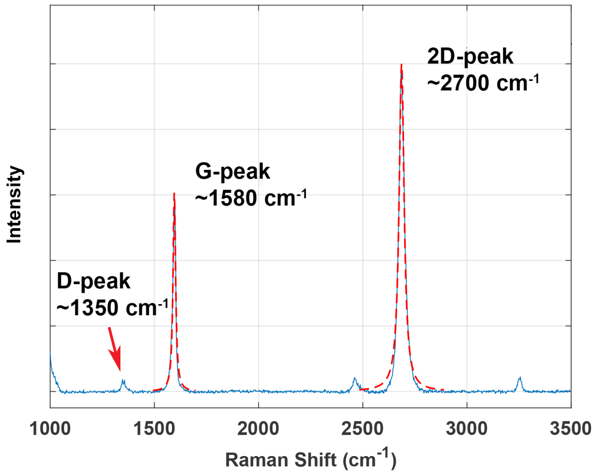

FIGURE 2.5: Schematic of a typical Raman spectrum indicating the position of the D, G and $2D$ peak.

Raman spectroscopy is often used and gives a reliable result[31], however a single Raman spectrum gives only information about the local measured spot. Therefore, another method to determine the number of graphene layers over a larger area by the optical transmittance of white light through graphene can be used. A single layer graphene experimentally absorps $\sim 2.3\%$ of incident white light[34]. Stacking multiple layers of graphene results in more absorption. The transmitted light $T(\omega)$ through such a stack of multilayered graphene can be described by equation 2.7[34] and is shown in figure 2.6.

$$T(\omega) = (1 + f(\omega)\pi\alpha N/2)^{-2} \tag{2.7}$$

with ω the wavelength of the transmitted light, $f(\omega)$ a correction coefficient , α a fine structure constant of $\sim 1/137$ and N the number of layers[34].

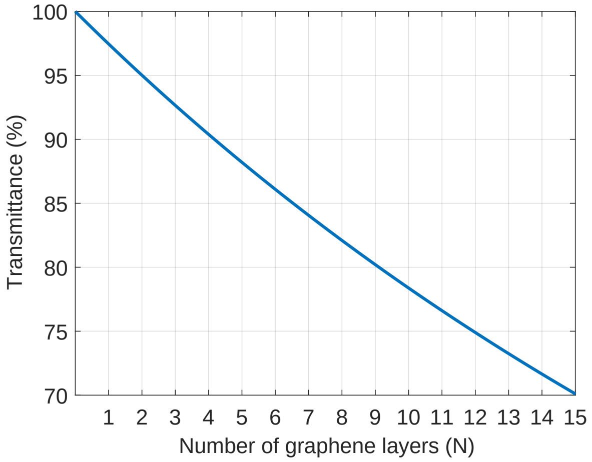

FIGURE 2.6: Optical transmittance of 550 nm light through N layers of graphene with correction coefficient $f(550\,\text{nm}) = 1.13$[34].

Optical transmittance measurements of visible light were planned to determine the number of graphene layers over a large area. However, the results are less reliable than hoped for. The findings and recommendations are displayed in appendix D. Fortunately, the performed Raman spectroscopy has validated the quality and the number of layers of the graphene as explained in section 4.1.1.

2.3 Transport theory

Multiple transport phenomena will be discussed. First of all, the bulk conductivity of an electrolyte is discussed. Subsequently, the transport in nanopores is examined. Thereafter, the significance of the surface conductance is discussed using the Duhkin number (Du). Furthermore, the possible influence of the electro-osmotic flow (EOF) is shortly discussed in appendix A.

2.3.1 Electrolyte conductivity

In order to move to the description of the resistor model in section 2.4 the basics of the conductivity of an electrolyte should be explained. The ability of an electrolyte solution to conduct electricity is called the conductivity κ and is often expressed as siemens per meter (Sm^{-1}). The conductivity of the bulk solution κ is for strong electrolytes, like KCl, composed of all the individual contributions of the ions following Kohlrausch's Law. This means that strong electrolytes are completely dissociated in the electrolyte and become directly proportional to the concentration at sufficiently low concentrations. For 1 M KCl the conducitivity is $\kappa = 11\,\mathrm{Sm}^{-1}$[35].

The conductance of microchannels is not only dependent on the electrolyte conductivity κ of the system, but also on the geometry. For example, in a 1D model the resistance can be modeled as[23]:

$$R = \frac{L}{\kappa A} \tag{2.8}$$

with L the length of the channel and A the cross-sectional area. In section 2.4 a disc geometry is introduced to describe the conductance of the formed blister between the graphene and SiN substrate.

2.3.2 Ionic conductance in nanopores

The total ionic conductance through nanopores larger than $\sim 9\,\mathrm{nm}$[36] can be described by the contribution of the access resistance and the channel resistance of a nanopore as shown in equation 2.9[37], [38].

$$G_{\mathrm{pore}} = (R_{\mathrm{channel}} + 2R_{\mathrm{access}})^{-1} = \sigma\left(\frac{4w}{\pi d^2} + \frac{1}{d}\right)^{-1} \tag{2.9}$$

with σ the ionic bulk conductivity, w the substrate thickness and d the pore diameter. This equation is valid for highly concentrated solutions for which the surface conductance can be neglected[39]. Rewriting equation 2.9 the size of nanopores can easily be calculated from pore conductivity measurements. The relation between the pore conductivity G_{pore} and the pore diameter d is given in figure 2.7.

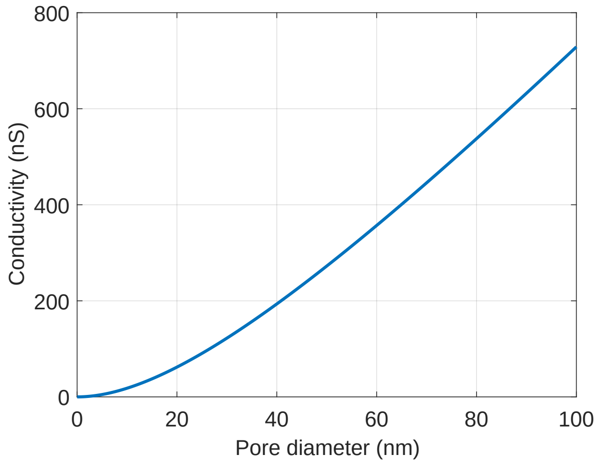

FIGURE 2.7: The pore conductivity versus the pore diameter in a 1 M KCl solution with $\sigma = 11\,\Omega^{-1}\mathrm{m}^{-1}$[35] and $w = 40\,\mathrm{nm}$.

2.3.3 Surface conductivity and the Dukhin number

The accumulation of surface charge at the interfaces leads to locally increased concentration and therefore conductivity, known as surface conductivity. In order to check if the surface conductivity has a significant influence on the transport in a system, the Dukhin number (Du) can be used. Du is a dimensionless quantity, which can be defined as the ratio between the surface and bulk conductivity, which boils down to equation 2.10.

$$\mathrm{Du} = \frac{\kappa_\mathrm{s}}{\kappa_\mathrm{b}} \tag{2.10}$$

For the purpose of this research Du can also be expressed as the Dukhin length l_Du using a Poisson-Boltzmann estimate to make a comparison between the surface to bulk conductance, which is often used in colloid science [39], [40]. l_Du is expressed in equation 2.11 and indicates at which channel dimensions the surface conduction, due to the surface charge density σ_s, plays an equal role to the bulk conductivity. This gives also insight in the transport phenomena in the graphene nanopores, which are in the sub 2 nm range.

$$l_\mathrm{Du} = \frac{|\sigma_s|/e}{2c} \tag{2.11}$$

The Dukhin length for 1 M KCl at a silicon nitride surface with a typical surface charge of $20\,\mathrm{mCm}^{-2}$[39] is $l_\mathrm{Du} = 0.1\,\mathrm{nm}$. The surface charge at a graphene interface with a transmembrane voltage of 1 V is $25\,\mathrm{mCm}^{-2}$[15] results in a comparable Dukhin length of $l_\mathrm{Du} = 0.13\,\mathrm{nm}$. With 1 M KCl electrolyte the graphene nanopore conductivity is most likely to be dominated by bulk conduction.

Moreover, from the presented Du lengths it is fair to assume that the surface conductivity in the graphene-electrolyte-SiN system is negligible compared to the bulk conductivity of the electrolyte at 1 M KCl. The height of the channel is expect to be several Deybe lengths ($\kappa^{-1} = 0.3\,\mathrm{nm}$).

2.4 Resistor model

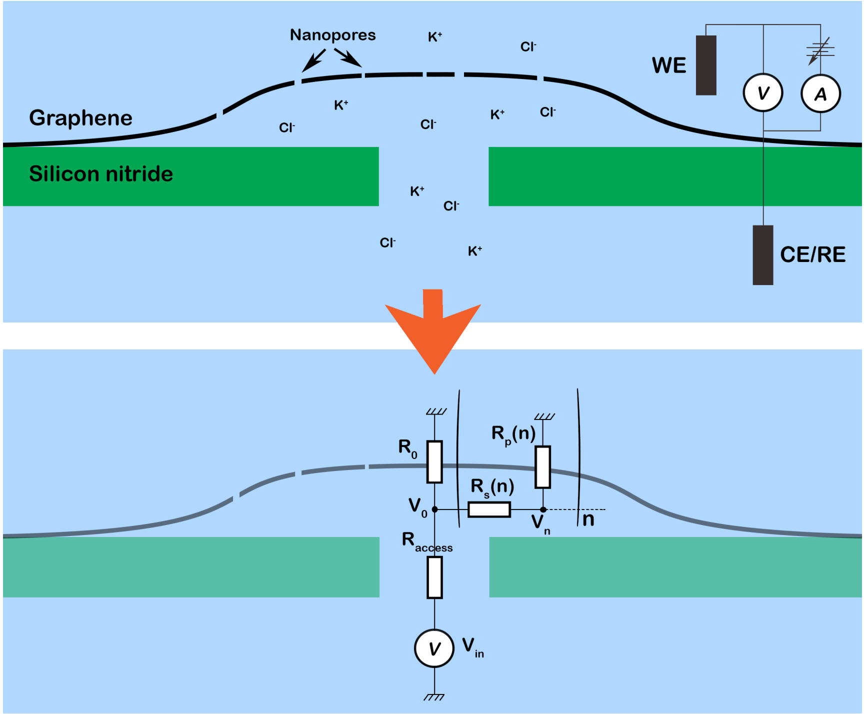

FIGURE 2.8: Schematic of the electrochemical system (top) translated to the proposed resistor model (bottom). The top schematic shows the detached graphene layer with small nanopores forming a blister on top of the SiN substrate. The bottom schematic depicts the implementation of the resistor model. The resistor chain R_s and R_p repeats n times, depending on the size of the blister. A new chain of resistors is added once the voltage at V_n exceeds the threshold voltage V_T and the blister extends.

In this section a resistor model will be introduced to give a simplified description of the physical system. The translation from the physical model to the resistor model is schematically shown in figure 2.8. The resistor model is developed to improve on several aspects of differential charge based transport models. The differential models consume a lot of computation time and use complex solvers, where as the resistor model is based on straight forward linear equations, which improve the simplicity and the computation time tremendously. The disadvantage of the resistor model is the simplification of the underlying physical transport phenomena.

The resistor model mimics electrowetting by an extending network of n resistors, as is shown in figure 2.8. Every time the voltage at the end of the network V_n exceeds the threshold voltage V_T, another instance of R_s and R_p is added. Furthermore, we assume that the formed blister is disc shaped as is shown in figure 2.9.

Resistor R_access is connected to the input voltage V_in and describes the access resistance of the SiN pore. The SiN pore is the limiting factor in the case that there is no graphene on top of the SiN membrane and will define the maximum conductivity of the system.

The next resistor, R_0, which is in series with R_access, defines the resistance of the graphene at $V_{in} =\sim 0\,\mathrm{V}$. At this potential there is no electrowetting so the initial resistance R_0 defines the resistance of the sheet of graphene directly on top of the

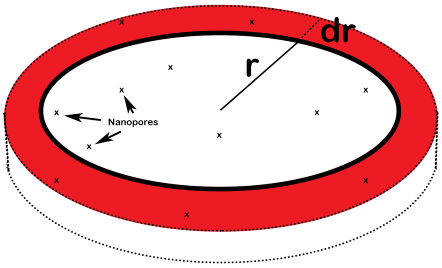

FIGURE 2.9: Top view of the blister's geometry for the resistor model. The disc extends with steps of n steps of dr, resulting in radius dependent values for $R_s(r_n)$ and $R_p(r_n)$.

SiN pore. In this situation it is most likely that one defect is exposed[1], [29]. R_0 is hundreds of times larger than R_{access}.

The moment that the graphene starts detaching at higher potential two new resistances can be defined. R_s defines the resistance of the bulk solution between the substrate and the graphene and R_{p} is the result of leakage through newly exposed nanopores in the graphene. The more graphene detaches from the SiN substrate, the more resistors are introduced to the system.

R_{s} and R_{p} are both subject to a form factor, because of the assumed disc shape in figure 2.9. From this point on the resistors are indicated as $R_{\text{s}}(r_n)$ and $R_{\text{p}}(r_n)$ to show their dependency on the radius of the disc as defined in equation 2.12 and 2.13. $R_{\text{s}}(r_n)$ is know as an annular resistance and can be calculated using an analogous heat transfer problem of heat conduction through a hollow cylinder with height h and conductivity κ. The derivation is shown in appendix B.

$$R_{\text{s}}(r_n) = \frac{\Delta V}{I} = \frac{1}{\kappa 2\pi h} \ln(\frac{r_{n+1}}{r_n}) \tag{2.12}$$

with r_n the radius of the blister, which is incremented by dr. $R_{\text{p}}(r_n)$ is prone to an expanding area as indicated in red in figure 2.9. The newly exposed area has a resistance which is related to the average defect resistance R_{d} and the defects spacing L_{d}, resulting in equation 2.13.

$$R_{\text{p}}(r_n) = \frac{R_{\text{d}} L_{\text{d}}^2}{\pi(r_{n+1}^2 - r_n^2)} \tag{2.13}$$

As mentioned before, the system expands when the following condition is met at the end of the expending resistor network: $V_T > V_n$. Every time the node voltage V_n exceeds the threshold voltage V_T, two extra resistors are added to the circuit. The circuit shown in figure 2.9 extends n times.

The electrical circuit is solved in MATLAB using a compact set of linear node-voltage equations. The node-voltage method is based on Kirchhoff's current law, which states that the sum of all branch currents at a node must sum to zero. In a network of N nodes, all constitutive branches are represented by an admittance matrix $\boldsymbol{G}$ of size $N \times N$. The node voltage matrix $\boldsymbol{V}$ has a size of $N \times 1$ and the source nodes are represented by $\boldsymbol{i}$ with dimensions $N \times 1$. The result is a set of of linear equations, which can be calculated by the matrix multiplication in equation 2.14.

$$\boldsymbol{G}^{-1}\boldsymbol{i} = \boldsymbol{V} \tag{2.14}$$

A MATLAB script is written to find the resistor network that satisfies the condition $V_T > V_n$ with the smallest n for a given V_{in} and thereby mimics electrowetting. The MATLAB script can be found in appendix C. The script works on a top level as follows:

1. Set system's initial conditions (e.g. V_{in} and $n = 0$)
2. Calculate resistor values for n expansion
3. Node-voltage equations solves network with n expansion
    - If $V_{\text{T}} < V_n$, increment n and go back to step 2
    - Else, go on to step 4
4. Return the node voltages, resistor values and number of expansion for the given initial conditions

Most system parameters can be estimated with the help of previous experimental data of W. van den Beld [1]. A 54 nm pore in the SiN layer without a graphene membrane has a conductance of $G_{\text{access}} = 329\,\text{nS}$, therefore the access resistance can be defined as $R_{\text{access}} = 1/G_{\text{access}} = 3\,\text{M}\Omega$. Furthermore, a system with the graphene membrane covering the SiN membrane has an average conductance of $G_{\text{system}} = 8\,\text{nS}$ at low voltage. At low voltages no wetting of the graphene sheet is expected, therefore R_{access} and R_0 in series define the total resistance of the system, resulting in $R_{\text{system}} - R_{\text{access}} = R_0 = 122\,\text{M}\Omega$.

To sum up, the model uses the following parameter values:

$r_0 = 27\,\text{nm}$

$h = 20\,\text{nm}$

$\kappa = 11\,\Omega^{-1}\text{m}^{-1}$[35]

$R_0 = 122\,\text{M}\Omega$

$R_{access} = 3\,\text{M}\Omega$

$dr = 1\,\text{nm}$

$L_{\text{defect}} = 70\,\text{nm}$

$R_{\text{defect}} = 200\,\text{M}\Omega$

$V_{\text{T}} = 0.2\,\text{V}$

The model is validated using a few simulation results as shown in figure 2.10. In general, a clear change in conductivity is observed at the threshold voltage. The size of the blister rapidly expands at the threshold voltage and then the expansion reduces with increasing voltage. Different step sizes dr show that a minimum step size of 1 nm is required to get a result, which is independent of the step size. Furthermore, the channel height h has a significant influence on the curvature of the IV-curve and the maximum conductivity.

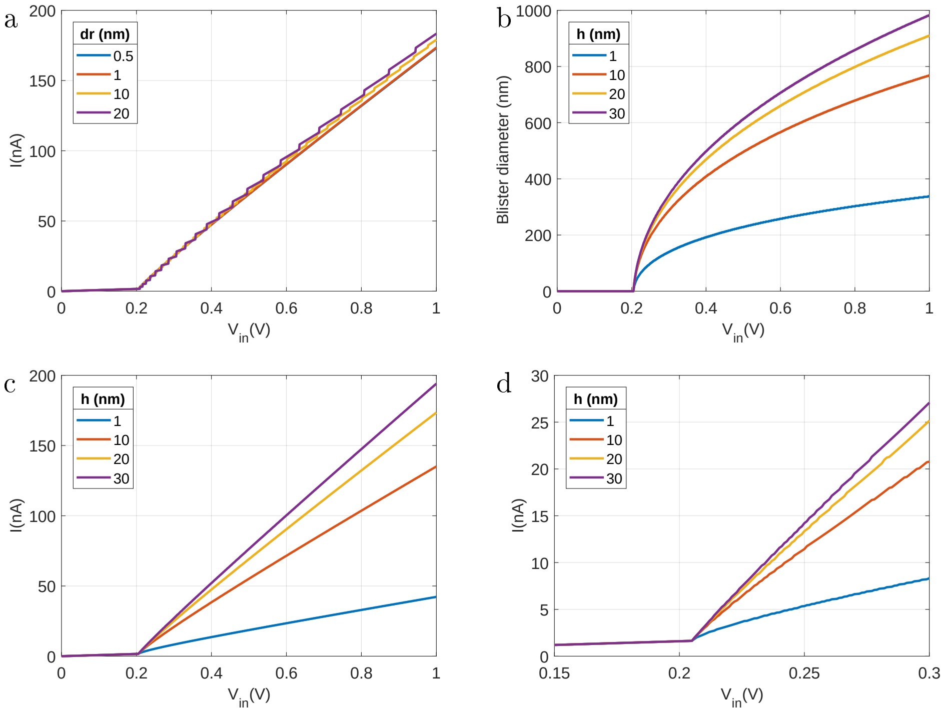

FIGURE 2.10: Simulation results of the resistor model in MATLAB. (a) shows the influence of the simulation step size. The blister diameter is plotted in (b) versus the input voltage for different channel heights. (b) indicates the influence of different channel heights on the IV-behavior and (d) is a zoom in to show slightly different curvatures.

The dependency of the model on the SiN nanopore conductivity R_{access} and the initial conductance through the graphen R_0 are shown in figure 2.11. R_{access} strongly dominates the maximum current in the system and R_0 influences the threshold voltage at which the system shows an increased conductivity.

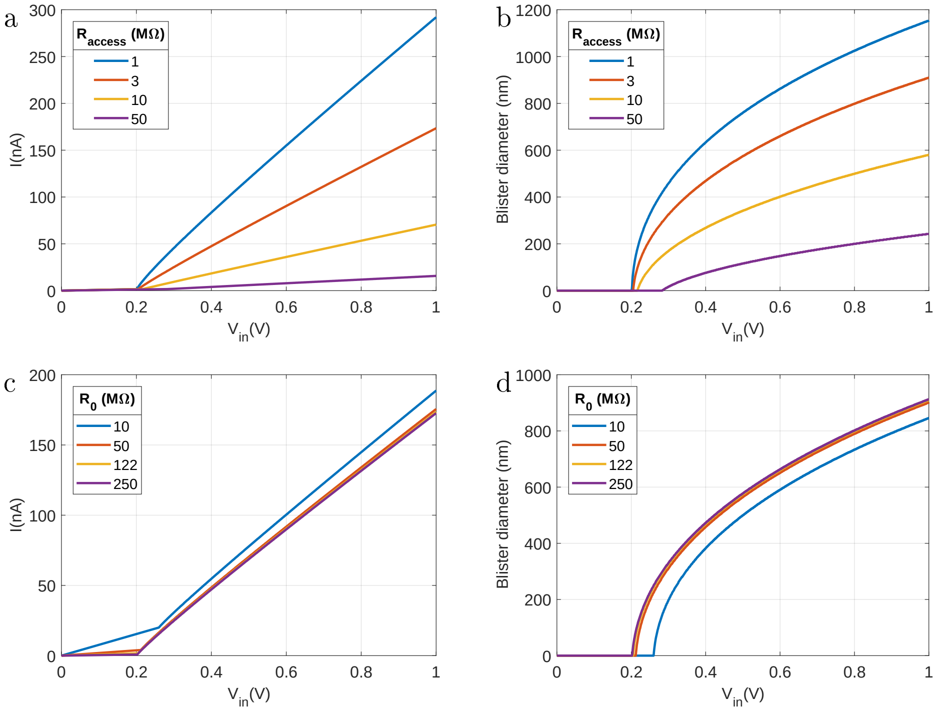

FIGURE 2.11: More simulation results of the resistor model in MATLAB. The access resistance of the SiN nanopore R_{access} and the initial resistance R_0 of the graphene are varied.

2.5 Electrochemistry

Electrochemistry is the science of interaction between electricity and chemical changes. When a potential is applied in the system shown in figure 2.12, an electron current flows in the electron-conducting wires, but free electrons cannot flow through the solution. Instead, the electron current will be converted to ion currents at the electrodes by oxidation-reduction (redox) reactions. Redox reactions are reactions in which electron transfer occurs between the electrodes and the electrolyte. Though redox reactions are needed at the electrodes to convert an electron current into ion currents, the current in the solution will be carried by all the ions present, and not only the ones produced at the electrodes by the redox reactions. The electron current is both measurable and controllable using a potentiostat, giving insight in the electrochemical reactions in the system. The basic elements of an electrochemical cell are illustrated in figure 2.12.

Electrochemical measurement techniques give a lot of information about the state of the cell. It reveals for example the conductivity in the system. This can be used to check the open pore conductivity of the SiN membrane or detect a leaky system. Four electrochemical measurement techniques are shortly discussed: open circuit voltage (OCV), chronopotentiometry (CP), chronoamperometry (CA), cyclic voltammetry (CV) and potentio electrochemical impedance spectroscopy (PEIS).

The open circuit voltage (OCV) measures the potential over the electrodes without applying any potential or current as if no external load is connected. It returns the difference in electrical potential between the electrodes.

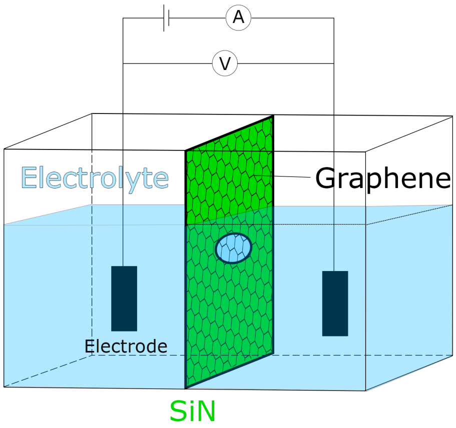

FIGURE 2.12: Illustration of an electrochemical cell with two electrodes in an electrolyte separated by leaky graphene on top of a SiN membrane. The electrodes are connected to a potentiostat, which controls and measures the voltage and current in the cell. The left electrode is the working electrode (WE) and the right electrode is the counter and reference electrode (CE/RE).

Chronopotentiometry (CP) controls the current in the electrochemical cell and monitors the resulting potential. Usually a constant current is applied. A redox reaction at the working electrode is forced to supply for the current. CP gives information about the conduction path in the cell.

Chronoamperometry (CA) applies a constant potential at the working electrode, which results in a monitored faradaic current at the electrode. The faradaic current decays exponentially over time. The decay gives information about the resistance and capacitance (RC) in the system. Furthermore, the stabilized current is a measure for the conductivity of the system at a fixed potential.

Cyclic voltammetry (CV) is a potentiodynamic electrochemical measurement using a linear potential ramp in time. CV produces a current-voltage (IV) diagram as shown in figure 2.13, which gives information about the capacitance and conductance in the measured electrochemical cell as can be deduced from equation 2.15. The potential is ramped at a given scan rate $\frac{\mathrm{d}V}{\mathrm{d}t}$ over a given potential range. Following from this, the slope of the IV-curve is a measure for the conductance and the difference in current at a certain voltage is a measure for the capacitance in the system.

$$I = C\frac{\mathrm{d}V}{\mathrm{d}t} + \frac{1}{R}V \tag{2.15}$$

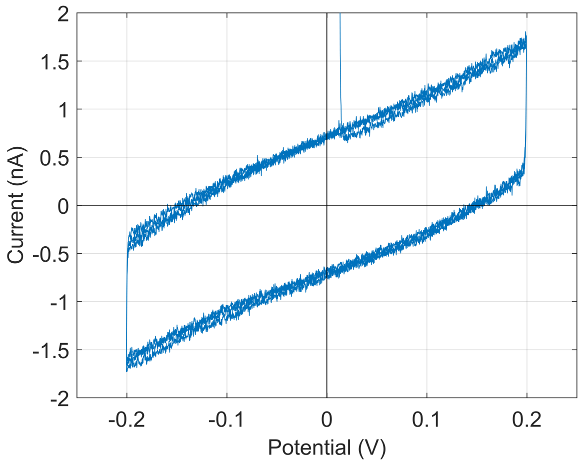

Figure 2.13: Example of a basic CV measurement. The slope of the IV-curve is a measure for the conductivity in the system and the difference in current at a certain voltage is a measure for the capacitance.

Potentio electrochemical impedance spectroscopy (PEIS) measures the frequency response of the electrochemical cell, giving information about the resistances and capacitances in the system. A low alternating potential is applied to the working electrode and the frequency of the signal is swept over a large range.

Chapter 3

Method

3.1 Graphene growth, transfer and characterization

Monolayer graphene is grown on copper using chemical vapor deposition (CVD). Thereafter the grown graphene is transfered to a SiN substrate or to a silicon dioxide substrate for characterization. Raman spectroscopy is a convenient method to determine the number of grown graphene layers and the Raman spectrum gives information about the quality of the graphene as well. However, a Raman spectrum only gives local information of the measured spot, therefore a scan over a larger area is performed. Unfortunately, the planned transmittance measurements were not reliable. The process and results are explained in appendix D.

3.1.1 Growth

Monolayer graphene is grown in collaboration with E. Grady at the Plasma & Materials Processing (PMP) department of Eindhoven University of Technology. The graphene is synthesized on copper by means of low pressure chemical vapor deposition (LPCVD). The low solubility of carbon in copper helps the self-limiting surface-catalyzed growth process[41]. LPCVD is advantagous compared to atmospheric pressure chemical vapor deposition (APCVD), because the graphene growth is self-limiting for LPCVD independent of the methane concentration, which is not guarenteed for APCVD[42]. The described graphene synthesize is based on the previous work and expertise of W. van den Beld and E. Grady[1].

A top level description of the growth is given in this section and the details of the growth process and materials are given in appendix E. The used CVD furnace of the PMP department is shown in figure 3.1. Copper foil is used as catalyst material and is loaded on the quartz boat, which can be slit into the quartz tube. The furnace can be slit onto the tube. Prior to the loading, the copper sheets are cleaned with acetone, methanol and nitric acid. In the meantime the furnace is heated to 1050 °C and the quartz tube is purged with argon gas. Thereafter, the tube is pumped down to low pressure. Next, the furnace is moved over the quartz tube and the copper is annealed at high temperature. Lastly, the graphene is grown by introducing an additional methane flow to the tube at the same high temperature.

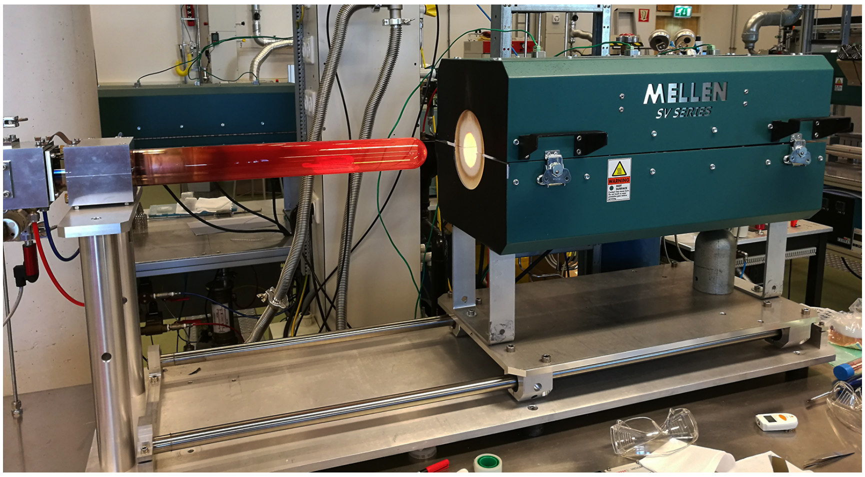

FIGURE 3.1: The setup shows the CVD system of the PMP department at the Eindhoven University of Technology a few seconds after the quartz tube is removed from the furnace. The quartz tube on the left contains a quartz boat onto which the copper foil is loaded. The furnace on the right can be slide onto the tube.

3.1.2 Graphene transfer

The CVD grown graphene must be transferred from the copper catalyst to a substrate. A transfer protocol from W. van den Beld[1] is adapted for this purpose. The detailed transfer protocol can be found in appendix H. A brief description follows and is supported by the process flow in figure 3.2.

At first, a polymer layer of ∼ 100 nm PMMA is spin coated on top of the graphene and pre-baked for support during the transfer. Next, the graphene is cut with a scalpel into small square pieces of ∼5x5 mm. The back-side of the graphene is then removed by nitric acid and subsequently the copper is etched overnight in low concentrated ammoniumpersulfate (APS). The graphene transfer to a substrate is done by scoping the graphene from a water vortex. The water vortex rinses the graphene and removes the copper etch. Subsequently, the graphene-PMMA layer on top of the substrate is post-baked to form the PMMA to the SiN substrate. Finally, the PMMA is dissolved with acetone and the SiN-graphene device is left over.

The graphene is transferred to a silicon chip with a ∼ 40 nm thick silicon nitride (SiN) membrane on top. The silicon chip is back etched, such that a 80x80 µm SiN membrane is left over in the middle of the chip as illustrated in figure 3.3. The membrane contains an ion laser beamed hole of approximately 50 nm. The characterization of the nanopore in the bare SiN membranes are depicted in table G.1 in appendix G. The position of the ion beamed hole can deviates several tens of nanometers from the membrane's center. The fabrication process of the SiN membranes is described in the work of van den Beld[1].

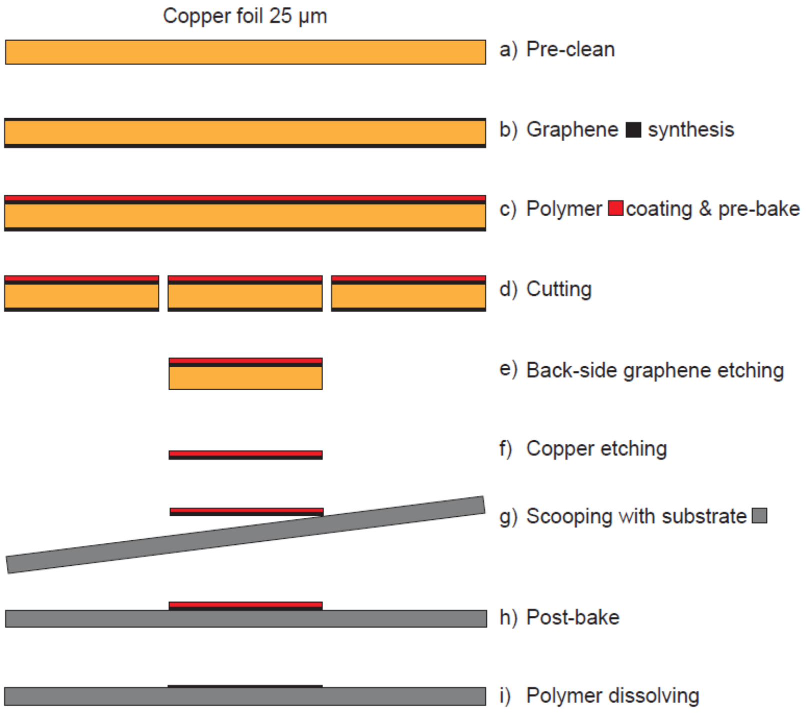

FIGURE 3.2: Schematic of the graphene transfer steps. The schematic is with permission used from [1]. Steps (a) and (b) illustrate the graphene synthesis as described in the previous section 3.1.1. After the synthesis the graphene is coated with a polymer for support and pre-baked (c). Subsequently, the graphene is cut in dices (d) and the back-side of the graphene is etched (e). Then the copper is etched (f), such that a layer of graphene supported by a polymer is left over. The graphene is scooped on the substrate (g) and post-baked (h). Finally, the polymer is dissolved and the graphene on top of a substrate is left over (i).

FIGURE 3.3: Schematic of the SiN membrane (green) with the ion laser beamed hole on top of silicon (orange). The left figure shows a cross section and the right figure a bottom view. The scale does not correspond with reality.

3.1.3 Optical inspection

After the graphene transfer, the fabricated devices are optically examinated with a Leica DM6000 M optical microscope in reflection mode. The devices are checked on good graphene coverage, torn or folded graphene, contaminations and an intact SiN membrane.

3.1.4 Raman spectroscopy

Raman spectroscopy is used to determine the number of grown graphene layers and the quality of the grown graphene. A single Raman spectrum gives only information about a spot size of 0.72 µm. In order to check the local quality of the graphene on different locations 9 Raman spectra are recorded in an area of 10x10 μm^2 and processed using a MATLAB script. The details of the Raman setup, measurement settings and processing are described in appendix F.

3.2 Experimental setups

The electrowetting of the suspended graphene membrane on a SiN membrane is investigated using the device holders in figure 3.4. The closed device holder in figure 3.4a is used for electrochemical measurements in combination with robust saturated mercury electrodes (SCE). These two references electrodes can be used at low currents and have the advantage of a low resistance. The open device holder in figure 3.4b is used for in liquid optical and AFM measurements, which are performed in collaboration with Edwin Dollekamp of the Physics of Interfaces and Nanomaterials (PIN) department at the University of Twente. The holder most be open, because the graphene must be visible and accessible from the top. Small silver/silverchloride (Ag/AgCl) wires as electrodes are used in combination with the open holder, such that the optical microscope objective and the AFM nose cone can be positioned in the vicinity of the SiN-graphene interface. The synthesize of the Ag/AgCl electrodes is described in appendix J. In general, the SiN membrane covered with graphene separates two electrolyte reservoirs. For almost all experiments 1 M KCl is used unless stated differently. This is a typical electrolyte used for DNA applications with similar devices[2].

In order to observe optical changes at the SiN-graphene interface the feature size must be larger than $\sim 0.2\,\mu m$ [43]. Therefore, the optical resolution is too low to observe changes at 1 V. By trial, optical changes have been observed when CV measurements are run up to 2.5 V. Since the profile changes at lower voltage are also of great interested, additional AFM measurements in liquid are done at lower voltage. Besides that, AFM measurements verify that the observed changes in contrast are genuinely the result of graphene detachment on top of the SiN membrane. Furthermore, the optical measurements give information about the location of the blister. This is needed to perform an AFM scan in the proper area.

3.2.1 Electrochemical measurements

A series of electrochemical measurements are done to characterize the system and to obtain data about trans-membrane transport in the form of IV-curves. Before, the IV-curves of the system are recorded, the electrodes are calibrated by placing the electrodes in the same reservoir as elaborately described in appendix I.0.1. Subsequently, the electrodes are placed in different reservoirs to obtain information about the SiN-graphene interface. The details of the used electrochemical techniques are mentioned in the measuring protocol in appendix I.0.2.

Before the graphene is transfered to the SiN membranes, the bare SiN membranes are characterized in order to check if the ioned beamed hole in the membrane is well

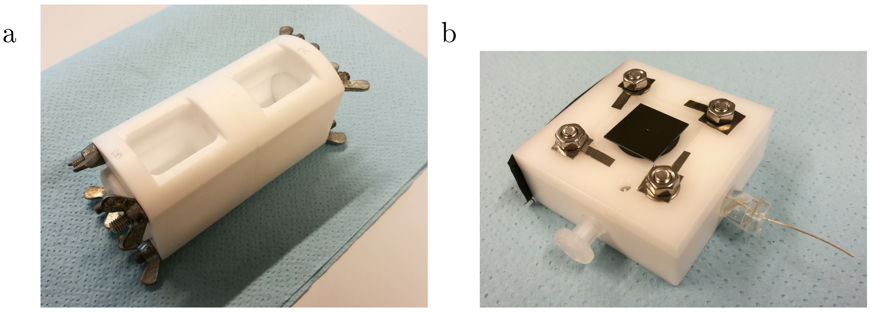

Figure 3.4: Two experimental setups are used: a closed device holder (a) and an open device holder (b). In the closed holder the device is positioned vertically between the two reservoirs. The device is clamped between two O-rings and the two reservoirs. The open holder has one reservoir below the device, which is addressed by the electrode that sticks out on the bottom right. It is important that the bottom reservoir is completely filled to make electrical contact. On top of the bottom reservoir an O-ring is placed with the device on top, which is pressed on the O-ring by spring steel clamps.

defined. This is done by obtaining the open pore conductance after a quick 2 min oxygen plasma treatment. The results are displayed in appendix G. Some of the SiN membranes are not used, because of their poor conductivity.

The first CV measurements on the graphene devices are run at low voltage from −200 mV to 200 mV. In this regime no electrowetting is expected, such that the measurements give insight in the graphene defects directly on top of the SiN pore. Secondly, experiments are conducted from −1 V to 1 V to get insight in electrowetting phenomena. Additional measurements are done at different salt concentrations. The measurements are conducted at ±200 mV, ±1 V and ±2.5 V for 1 mM KCl and 1 M KCl. These measurements give extra information on the influence of the EDL and therefore the surface conduction. The influence of the surface conduction is shortly demonstrated by measuring the conductivity of a bare SiN pore at 1, 10, 100 and 1000 mM.

The exact description of the electrochemical measurements and setup are given in the measuring protocol in appendix I.

3.2.2 In liquid optical reflection microscopy

Images are acquired while performing electrochemical measurements using optical reflection microscopy in liquid. The optical images reveal the exact location and shape of the formed blister. The first helps positioning the cantilever of the AFM in the next set of measurements. The used setup is shown in figure 3.5. For the electrochemical measurements the voltage range is increased to −2.5 V to 2.5 V in order to form a blister which is large enough to observe optically. To reduce the amount of produced data the CV measurements are run at a scan rate of 25 $\mathrm{mVs^{-1}}$.

The setup consists of a Leica DM2500 MH optical microscope with a 63x objective. The images are recorded using a PCO Pixelfly 14 bit digital CCD camera system. The microscope was operated in reflection mode. Data processing of the images is done using ImageJ. ImageJ is used to obtain the mean grayscale of the area near the formed blister. Each pixel has a value between 0 and 65.536 (16 bit). 0 zero is for black and 65.536 for white. The change in mean grayscale gives therefore information about color changes in the examined area.

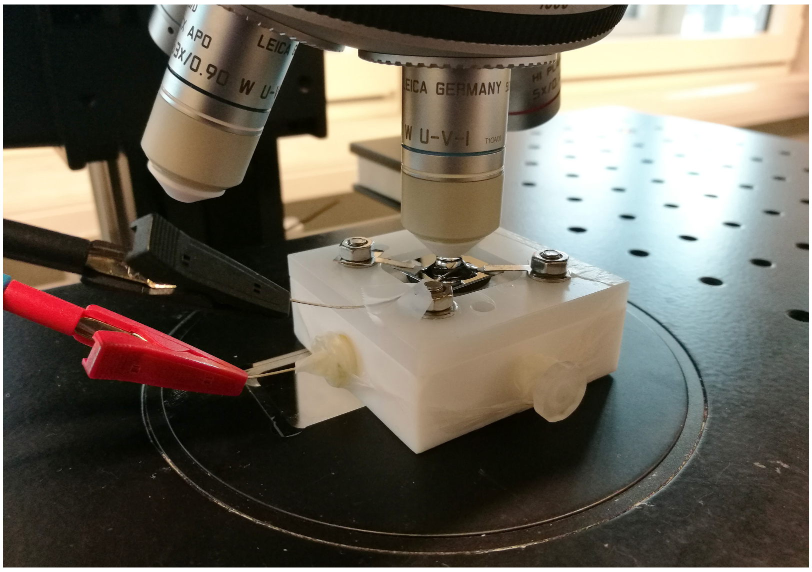

FIGURE 3.5: Optical reflection microscopy in liquid. The device holder has a closed reservoir with an Ag/AgCl wire introduced from the side (connected by the red clip). On top of the reservoir an O-ring is placed. The SiN chip is clamped on top of the O-ring with metal clamps. Another Ag/AgCl wire is placed on top of the SiN chip (connected by the black clip). A few milliliters of electrolyte are introduced on the top by a pipet.

3.2.3 In liquid atomic force microscopy

In liquid AFM is used to investigate if the graphene membrane is indeed electrowetting from the SiN membrane after a certain threshold voltage by measuring the height profile of the graphene. AFM allows measurement of height profiles by recording the deflection of a very small cantilever. The tip of this cantilever can be much smaller than the diffraction limit of light used in optical microscopes. A mechanical probe is introduced in the vicinity of the surface to obtain information. Tiny movements of the probe are controlled by piezoelectric elements and make the probe resonate. The probe experiences a force between the probe and the surface depending on the intermediate distance, which affects the deflection of the probe. Registering the deflection gives information about the height of the surface. Subsequently a surface profile can be obtained by scanning the surface over a larger area.

The setup in figure 3.6 is used for the AFM measurements in liquid. The sample is approached from the top by the AFM tip and the tip is emerged in liquid. The AFM nose cone had to be electrically isolated from the rest of the AFM system to prevent interference with the Ag/AgCl electrode in the same electrolyte reservoir.

A single AFM scan takes several minutes, therefore the potential is kept constant using CA for tens of minutes. At each constant potential three subsequent AFM scans are done and the induced current is recorded at the meantime. After each set of scans at constant potential a reference scan is done at 0 V to check if the blister disappears again. Measurements at the following potentials are conducted: 0, 0.5, 1.0 and 1.5 V.

Measurements were performed with an Agilent 5100 AFM in tapping mode. A NSC35a AFM tip from MikroMasch with a typical resonance frequency of 205 kHz and a force constant of 8.9 $\mathrm{N m^{-1}}$ is used. Images are collected with a resolution of 512 measurement points per line at 2 Hz over an area of 20x20 µm. The AFM data

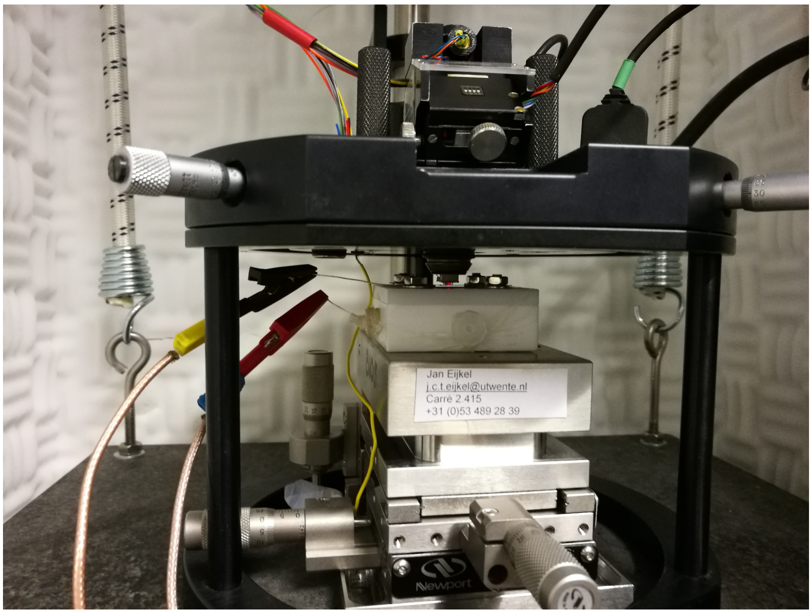

FIGURE 3.6: AFM setup with the open sample holder. An area of 20x20 µm^2 is scanned, while a constant potential is applied.

is processed using Gwyddion. Mean plane substraction and polynomial background removal are used to level the data.

Chapter 4

Results and discussion

The characterization of the graphene and the fabricated devices will be discussed first. Thereafter, the experimental work will be discussed. Table 4.1 gives an overview of all the experiments on the graphene devices that are discussed in this chapter. Optical and AFM measurements are performed on device 1 during electrochemical measurements, whereas device 5 is only optically examined during electrochemical measurements. The results prove the detachment of the graphene from the SiN substrate.

TABLE 4.1: Overview of the discussed experiments on the graphene-SiN devices.

Method	CV	CV	CV	CV/Optical
Range	±200 mV	±1 V	±2.5 V	±2.5 V
Holder	Closed	Closed	Closed	Open
Scan rate	10 mVs^{-1}	10 mVs^{-1}	10 mVs^{-1}	25 mVs^{-1}
Device				
1	x			x[2]
2	x	x		
3	x	x		
4[3]				
5				x
6	x[1]	x[1]		
7	x[1]		x[1]	

[1] also tested at low salt concentration. [2] AFM measurments. [3] Broken SiN membrane.

4.1 Characterization

In this section the quality of the CVD grown graphene is determined by interpreting the Raman spectra. Furthermore, the graphene transfer to the SiN membrane is optically evaluated.

4.1.1 Raman spectroscopy

The results and analysis of the Raman spectroscopy are shown in figure 4.1. The Raman spectra of the scanned area indicate monolayer graphene: the $I_{2\mathrm{D}}/I_{\mathrm{G}}$ ratio is larger than 1 for most measurements as can be seen in figure 4.1b; the fitted FWHMs of the $2D$-peak depicted in figure 4.1c are small and comparable to literature[31]. Furthermore, the negligible D-peak in figure 4.1a suggests good quality graphene with little defects. The Raman spectra for all measured spots are shown in appendix F. The results are consistent over a large area, such that it is fair to assume the graphene is monolayer and of good quality.

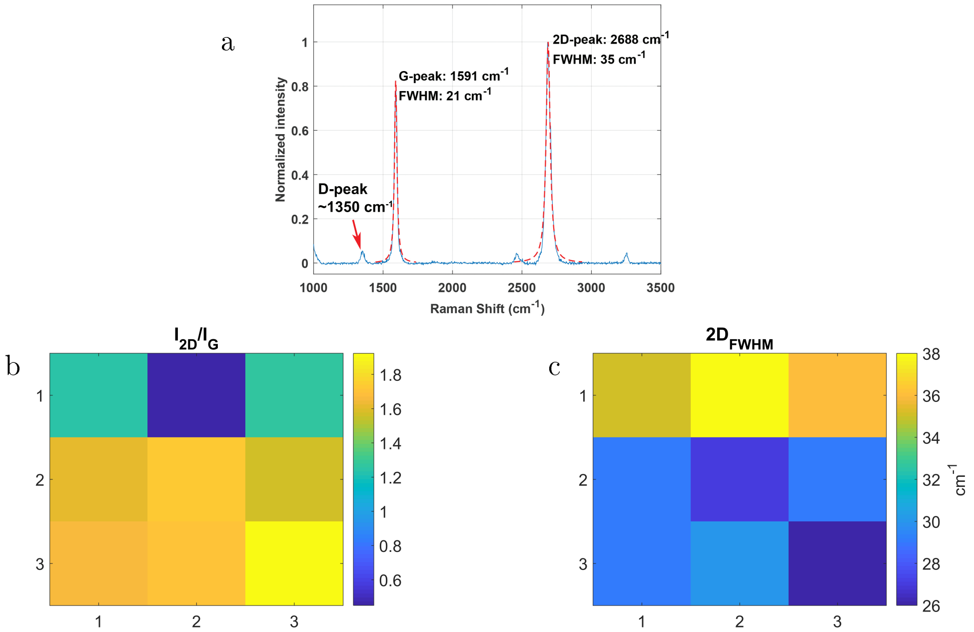

FIGURE 4.1: Raman analysis of a 10x10 µm^2 scanned area with 9 measurement points. The Raman spectrum for position (1,1)(a) shows a negligible *D*-peak. The I_{2D}/I_G ratio is larger than 1 for most measurements (b). The *2D*-peak FWHMs (c) are comparable to values found in literature for monolayer graphene.

4.1.2 Optical inspection

Optical images of two devices are shown in figure 4.2. Both images show good graphene coverage of the thin SiN membrane (light blue). Graphene wrinkles on the thin membrane can be observed in white. These wrinkles are formed, due to a difference in thermal expension coefficient of copper and graphene. The induced residual strain is released by the formation of wrinkles[41], [44]. Furthermore, the wrinkels are expected to be folded, since only wrinkles with a maximum height of ∼ 6 nm are standing[45], [46] and the feature size of the observed wrinkles are much larger.

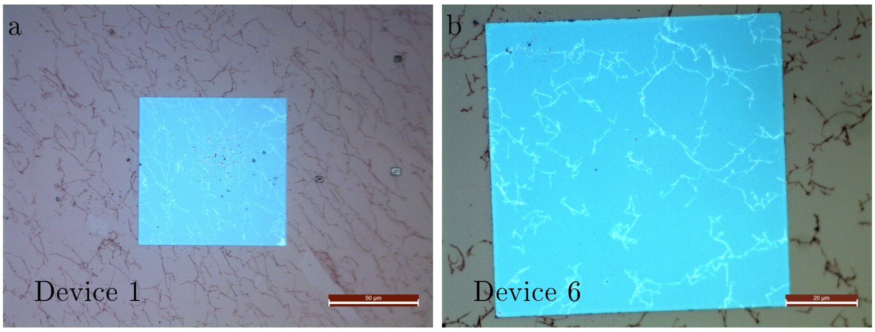

FIGURE 4.2: Optical image of devices 1 (a) and 6 (b) with respectively 50x and 100x magnification. The SiN membrane appears light blue and the graphene wrinkles are white. Both membranes are covered by graphene wihout tears. Some contaminations are visible as dark spots.

4.2 Electrochemical measurements

4.2.1 200 mV CV measurements

CV measurements are performed from −200 to 200 mV on several devices as can be found in appendix K. At these low voltages we do not observe any evidence of electrowetting, so the IV-curves are assumed to only give information about the conductivity of the defects that are directly on top of the SiN pore. Jain *et al.*[29] have shown a relation for the defect diameter versus the conductance using molecular dynamics simulations, which are backed with experimental results. These findings are used to give expression to the intrinsic defects of the 5 tested devices as can be seen in table 4.2. The assumption is made that only one defect is exposed, which is a fair assumption if the defect spacing is 70 nm to 100 nm, as expected from the literature[29], [30]. The found defects sizes range from 0.85 nm to 2.4 nm.

TABLE 4.2: Characterization of graphene-SiN devices at low voltage in 1 M KCl.

Device	Conductance (nS)	Defect diameter (nm)
1	1.3	0.85
2	1.9	0.9
3	6	1.5
6	15	2.4
7	14	2.3

Most of the IV-curves in appendix K show a linear behavior in contrast to Jain *et al.*, who also observed more pronounced rectified and activated behavior[29]. The deviation may be explained by differences in the device fabrication protocol, which result in slightly different properties of the graphene defects. Another explanation is our small sample size. Only a fraction of Jain's devices showed the nonlinearity and we may not have tested enough devices to observe the same behavior. Furthermore, the measurements of Jain *et al.* show no capacitive effects, because their measurement method is slightly different. In their experiments, a 60 s delay is added after each voltage step before the current measurement is done, so that the charging effect of the capacitance is negligible.

The capacitance of the devices is calculated using equation 2.15. The difference in current at 0 V is on average roughly 1 nA at a scan rate of 10 mVs^{-1}, resulting in a capacitance of 0.1 µF. This is approximately accounted for by the capacitance of the silicon chip using the dielectric constant of silicon ($\epsilon = 12$[23]) and the chip thickness of 300 nm. The capacitance of the silicon chip is dominant in the system, because of the huge surface area compared to the SiN membrane. The capacitance of the silicon chip described as a double plate capacitor enclosed by the $\sim$ 12.42 mm O-ring is $\sim$ 0.4 µF, which is in the same order of magnitude as the measured capacitance of 0.1 µF.

4.2.2 1 V CV measurements

Another set of CV measurements is performed on 3 devices, however this time with a larger voltage window to observe electrowetting effects. The results are displayed in figure 4.3. All 3 devices show a different and very rich behavior. Each device is discussed and the curiosities are mentioned.

In general, the maximum current increases with every cycle for all devices. A possible explanation is the change in adhesion energy once a fresh piece of graphene detaches, due to the introduction of salt at the surface.

Device 2 clearly shows a lower conductance close to 0 V for each cycle, which is comparable to the conductance of the device without any electrowetting effects. At higher voltage an increased conductivity is observed, which can be explained by electrowetting. This claim is supported by the optical and AFM measurement results on device 1 in section 4.3.1, which show the formation and disappearance of a blister related to the same IV-behavior.

The threshold voltage at which electrowetting occurs on device 2 is reduced after the first time it is observed. Once the graphene is detached, salt from the electrolyte can adsorb or desorb to the exposed surfaces, possibly altering the surface chemistry and with that the adhesion energy. Furthermore, the device shows hysteresis in the positive voltage domain. The current is lower when the voltage is sweeping up compared to the current when the voltage is sweeping down. This may indicate that the graphene stays detached for a short while, even when the actual voltage is already below the threshold voltage for electrowetting. This might indicate a very weak attractive force that attracts the graphene back to the SiN substrate or a mechanical time delay is involved.

Device 3 shows in the first cycle an increase in conductivity at $\sim 0.2\,\mathrm{V}$, where after the conductivity is also increased at voltages much closer to 0 V. This could indicate that the formed blister, does not completely disappear once it is formed. As a result more defects are also exposed at low voltage. Reasons could be mechanical deformation in the form of buckling of the graphene. The same IV-behavior is observed for device 5 and optical measurement in section 4.3.1 have confirmed the deformation of the graphene.

For device 6 there is no significant increase in conductivity with voltage. However, the signal does show some disturbances. One possible explanation is that exactly on top of the pore the graphene is wrinkled or folded, which prevents the graphene from detaching. Another possible explanation may be the presence of a high conductivity intrinsic defect over the pore. As also observed in figure 2.11c, a high intrinsic defect conductance shifts the voltage at which electrowetting occurs, because the voltage across the graphene is lower.

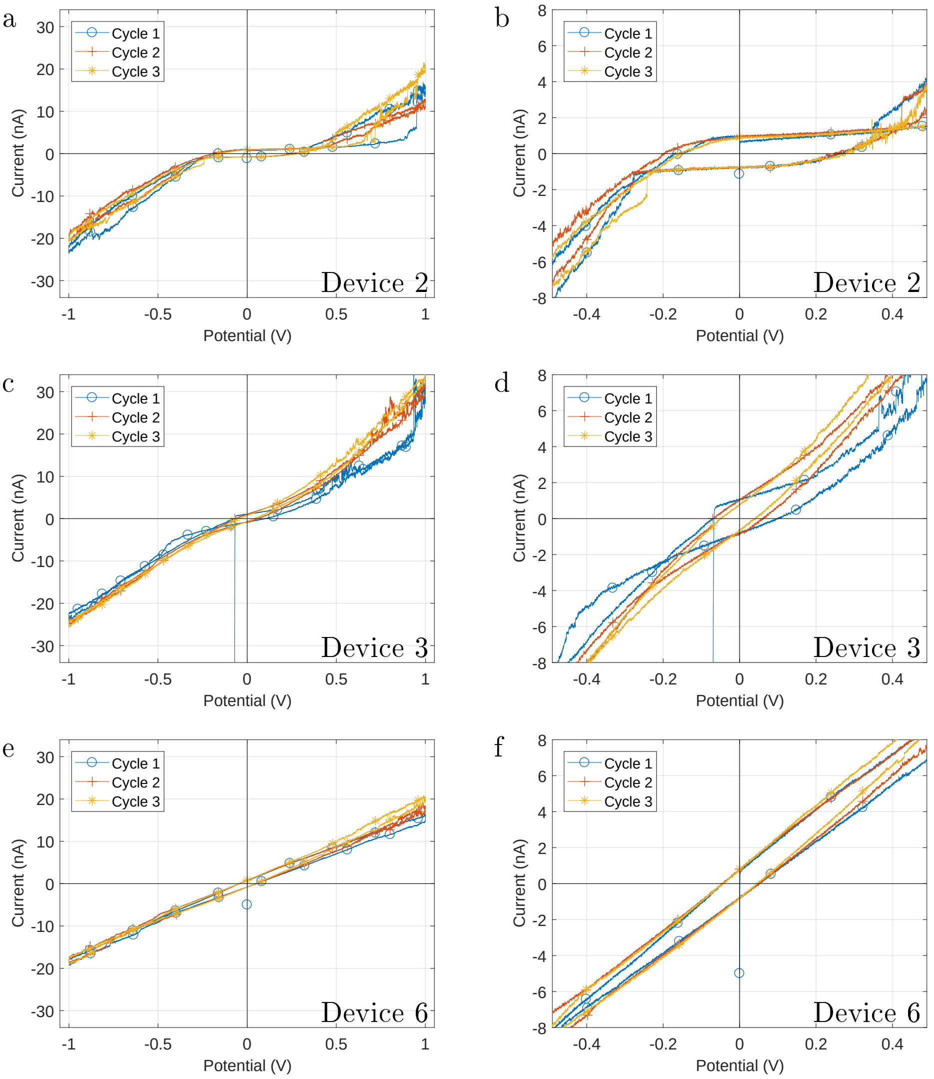

FIGURE 4.3: CV measurements in 1 M KCl for 3 graphene-SiN chips. The right column is a zoom in on the low voltage behavior. The CV measurements are run from −1 V to 1 V with a scan rate of 10 $\mathrm{mVs^{-1}}$.

4.3 Optical, AFM and electrochemical measurements

4.3.1 Optical reflection microscopy

The optical and electrochemical measurement results on device 1 are summarized in figure 4.4. The optical images show the folded graphene wrinkles in white. These wrinkles are stacked layers of graphene, which reflect more light. The same reflection is observed in the experiments and setup of Dollekamp *et al.*[43]. The same device reveals the formation of a dark spot when a large negative voltage is applied, as can be seen in figure 4.4a and 4.4b. The difference between the images is displayed in figure 4.4c. The dark spot subsequently disappears again at lower voltage. The dark spot is formed in the middle of the sample, as expected from the position of the SiN pore. Figure 4.4d shows the coincident CV measurement. The appearance of the dark spot is quantified by the mean grayvalue of the area around the dark spot. The grayscale is inverted, such that a peak occurs when the dark spot is formed. The occurrence and disappearance of the dark spot follows the voltage and the conductivity of the system as is shown in figure 4.4e and 4.4f. The dark spot is typically the largest, when the conductance is at its maximum. Furthermore, the system is asymmetric and shows a more dominant dark spot at negative voltages just like the CV. Unfortunately, there is spatial drift in the system, causing the focus to change over time. As a result the grayscale value drifts slighty over time.

The optical and electrochemical measurements in figure 4.5 summarize the results on device 5 in the same way as for device 1. The first blister is observed in the second cycle at positive potential. From that point on the blister does not disappear, which may be explained by the buckling of the graphene. The IV-curve linearizes at the last 1.5 cycle as can be seen in figure 4.5d. However, the conductivity seems to lag the inverse grayscale in figure 4.5f for almost a quarter of a cycle. The conductivity stabilizes in the second cycle at negative potential and approaches again the theoretical open pore conductivity of the SiN nanopore. To summerize, the detached graphene does not attach back to the SiN substrate around 0 V and the conductivity of the system is increased for all potentials.

The observed IV-behavior of device 5 is similar to the observed IV-behavior of device 3 in section 4.2.2 and confirms the suspicion that the buckling of the graphene may be a reason for the increase in conductance around 0 V.

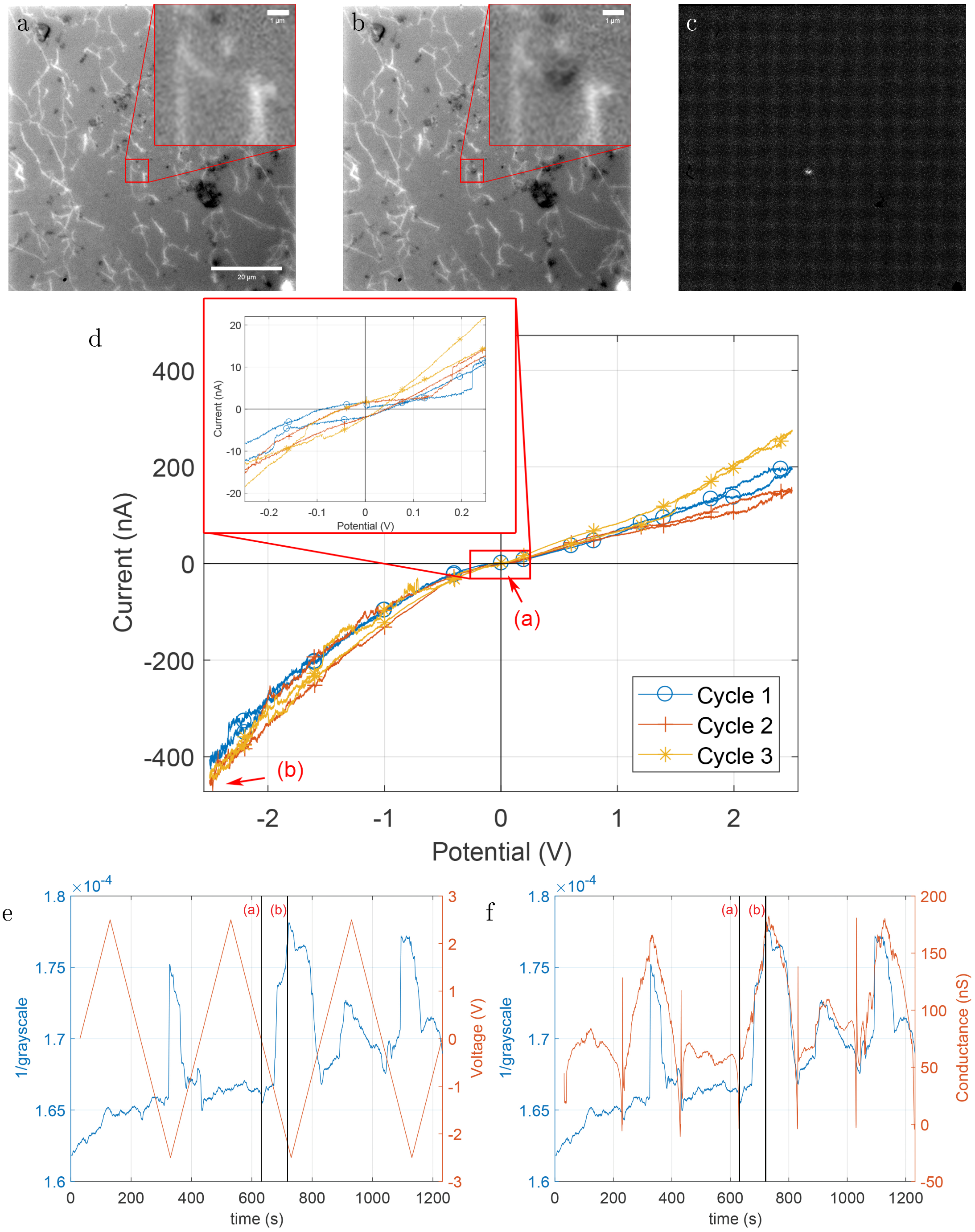

FIGURE 4.4: Optical image in liquid of the graphene on top of the SiN membrane of device 1 at 0 V (a). The optical image 100 s later at 2.5 V shows a black spot (b). The difference between image (a) and (b) is shown in (c). For the optical images the right bottom scale bar of (a) applies. The CV is run from −2.5 V to 2.5 V for 3 cycles with a scan rate of 25 mVs^{-1} (d). The voltage and inverse grayscale are plotted versus time (e). The images show a drift in grayvalue over time, due to spatial drift resulting in a changing focus. The conductance over time is found by CV measurements and correlates with the inverse grayscale (f). The conductance obtained from the CV shows spikes when the voltage switches polarity.

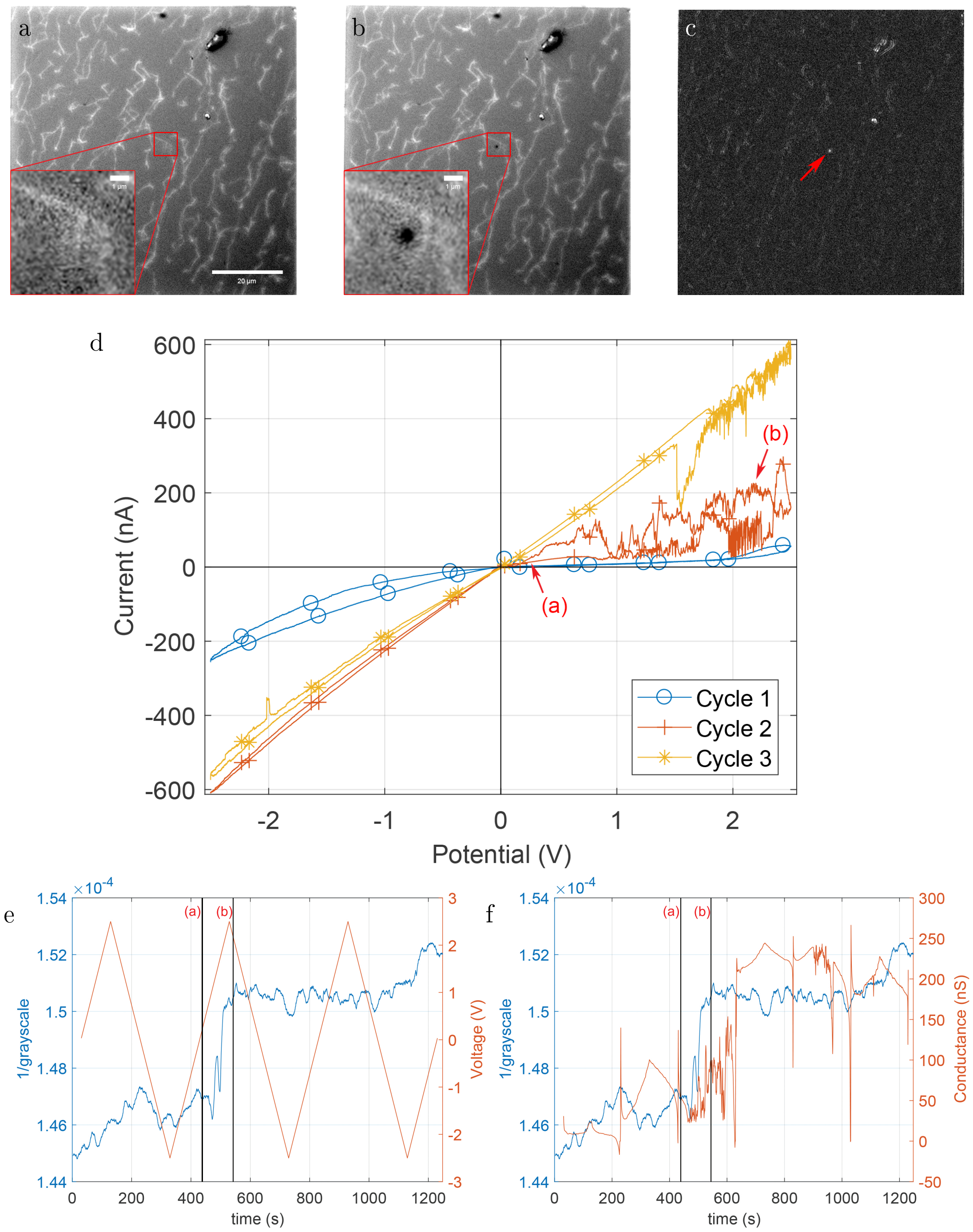

Figure 4.5: Optical image in liquid of the graphene on top of the SiN membrane of device 5 at about 0.2 V in the second cycle (a). The optical image later in the second cycle at 2.1 V shows a black spot (b). The difference between image (a) and (b) is shown in (c). For the optical images the bottom right scale bar in (a) applies. The CV is run from −2.5 V to 2.5 V for 3 cycles with a scan rate of 25 mVs^{-1} (d). The conductance over time is found by CV measurements and correlates with the inverse grayscale (e). The images show again a drift in grayvalue during the experiment, due to drift in the focus. The conductance obtained from the CV shows spikes when the voltage switches polarity.

4.3.2 AFM results

A comparison between the full AFM scan of 20x20 µm^2 and the optical image of the same area in figure 4.6a and 4.6b are shown. As expected the resolution of the AFM scan is much higher. Two AFM scans at a constant potential of 0 V and 1 V are displayed in respectively figure 4.6c and 4.6d. CV measurements are in this case not possible, because of the large time resolution of each AFM scan. The red square in the figures indicates the area of interest and is enlarged. The location is known from the previous optical measurements. The AFM scan at 1 V shows the occurrence of a blister as expected from the optical measurements.

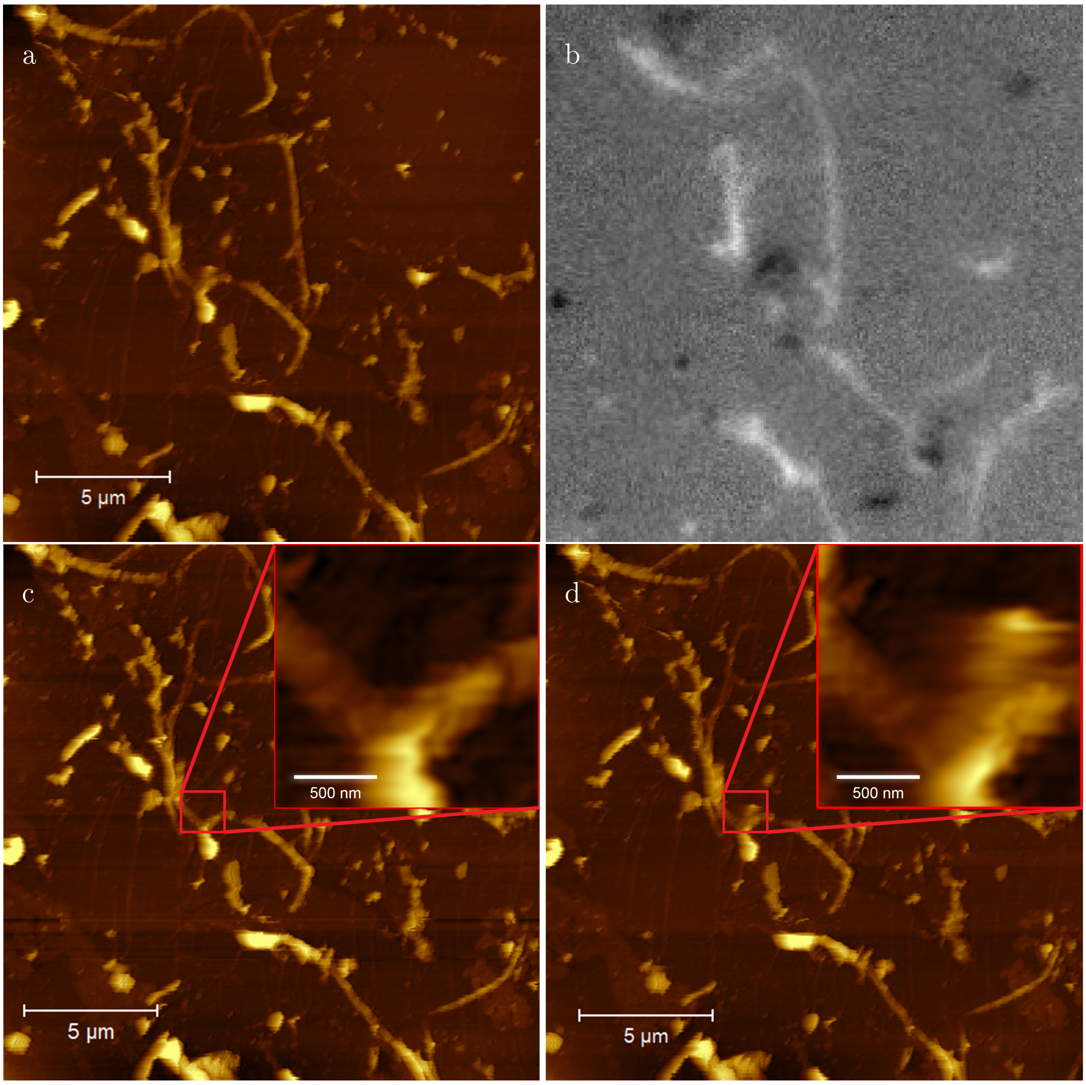

FIGURE 4.6: The comparison between the AFM (a) and optical measurement (b) are shown. The same scale bar applies. AFM scan at 0 V (c) and 1 V (d) showing the height profile of the graphene: the brighter the color, the higher. When a potential is applied (d) the formation of a blister is observed.

The close ups of all the consecutive AFM scans are displayed in figure 4.7. Every time a potential is applied, a blister is observed. The reference scans between the different applied potentials at 0 V shows that the blister has disappeared again.

Unfortunately, the device had to be reassembled after the second AFM scan at 1.5 V, because the device showed an unreasonable high current. The high current is the result of electrolyte creeping underneath the O-ring, which causes a new conduction path outside the device. After the reinstallment of the device the graphene was torn. This can be the result of pressing to hard with the AFM tip on the graphene.

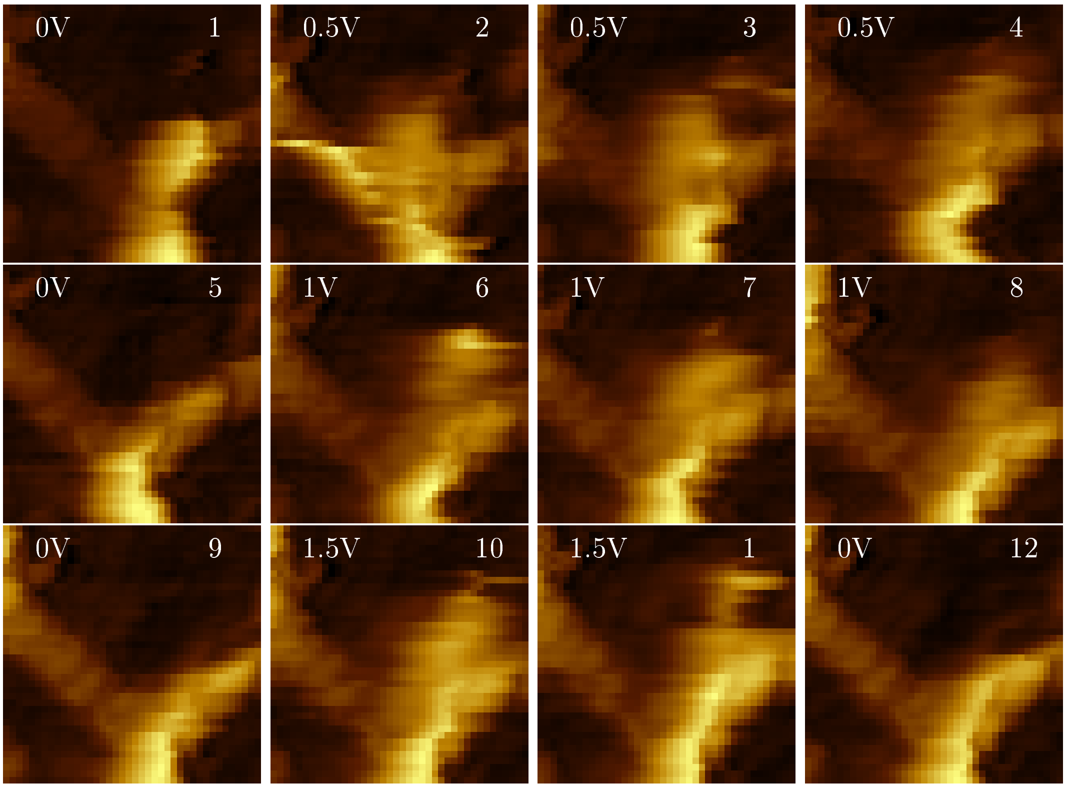

FIGURE 4.7: Close up of all AFM scans for different applied voltages. The intensities of the images are not the same. The number in the right corner indicates the order in which the measurements are performed.

It is difficult to obtain quantitative information of the formed blisters, because of the low resolution and the interfering wrinkle. The height profile of the measurement 2 and 7 are given in figure 4.8. The maximum height of the blister can be estimated at $\sim 30\,\mathrm{nm}$ and on average $\sim 20\,\mathrm{nm}$. Furthermore, the diameter deviates approximately between 500 nm and 1000 nm.

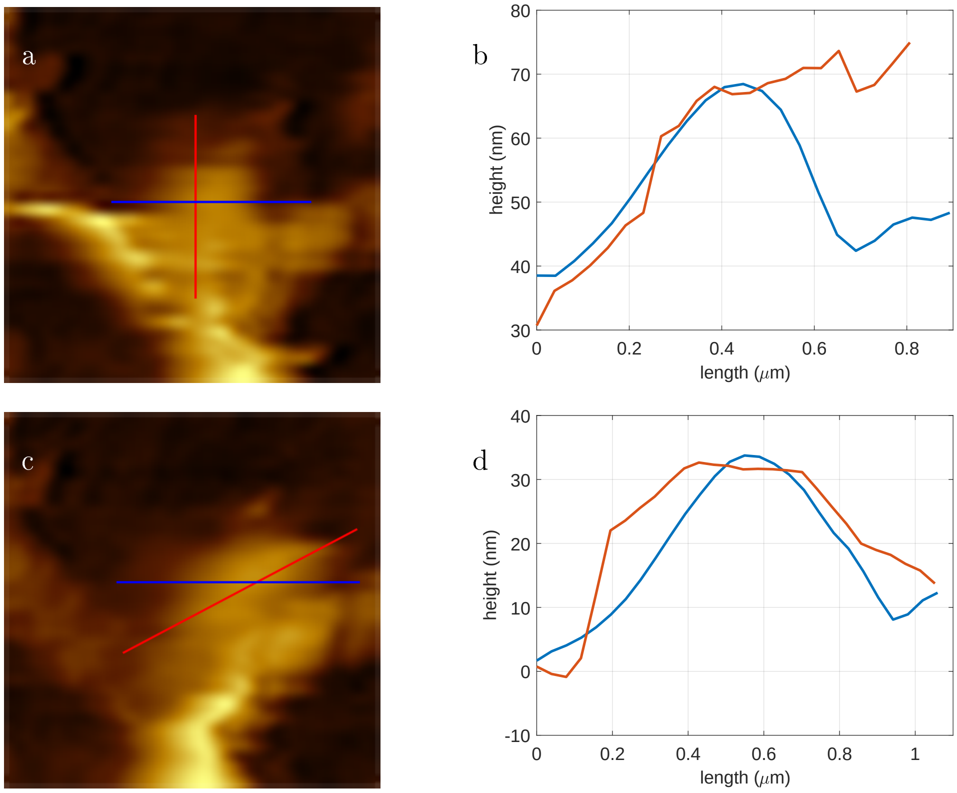

FIGURE 4.8: The height profile of the AFM scan 2 at 0.5 V (a) and scan 7 at 1 V (c) are plotted in respectively (b) and (d).

4.4 Model evaluation

The basic response of the model is evaluated using the experimentally determined parameters. The model parameters are set using the initial characterization, IV-response and AFM measurements from device 1 without fitting. The following parameters are considered:

$r_0 = 25\,\text{nm}$

$h = 20\,\text{nm}$

$\kappa = 11\,\Omega^{-1}\text{m}^{-1}$

$R_0 = 750\,\text{M}\Omega$

$R_{\text{access}}(\text{min}) = 8.5\,\text{M}\Omega$

$R_{\text{access}}(\text{max}) = 13\,\text{M}\Omega$

$dr = 1\,\text{nm}$

$L_{\text{defect}} = 70\,\text{nm}$

$R_{\text{defect}} = 200\,\text{M}\Omega$

$V_{\text{T}} = 0.2\,\text{V}$

The model is compared to the experimental data in figure 4.9. The access resistance is based on the minimum and maximum conductance in the positive voltage regime of the CV measurement, as can be found in figure 4.4f. The current fits very well with the CV measurements. Furthermore, the order of magnitude of the predicted blister diameter is also consistent with the experimental data of the AFM (0.5 µm to 1 µm) and the optical microscopy (∼ 1.5 µm). To sum up, the basic physical behavior of the system can be approached by the resistor model.

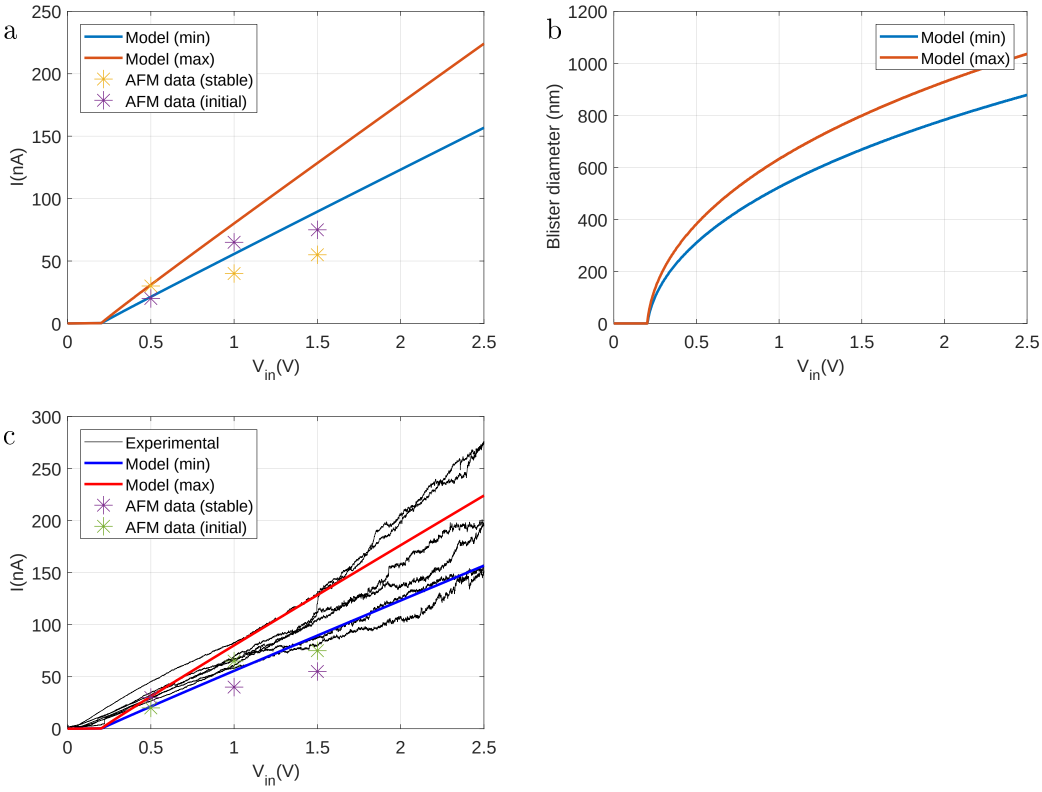

FIGURE 4.9: A comparison between the resistor model and experimental data is made. (a) compares the model to the measured current during the AFM measurements. A distinction is made between the initial current, when the potential is applied and the stable current after some time. The diameter of the blister according to the model is shown versus the voltage (b). The IV-curves measured during the optical measurements are displayed as well (c).

4.5 Low salt measurement

The following measurement results are preliminary results to illustrate the influence of the salt concentration on the dynamics of the system.

The first set of measurements focus on the influence of the surface conductivity on the total conduction in a nanopore. The conductivity of a bare SiN nanopore with no graphene at different KCl concentrations is shown in figure 4.10. The pore diameter is deducted from equation 2.9 and leads to a diameter of 70 nm. Theoretically, as expressed in equation 2.11 the surface conduction becomes dominant at 3 mM. This is in line with the relatively high conduction observed at 1 mM where the linear trend of the ionic bulk conductivity versus the concentration is broken.

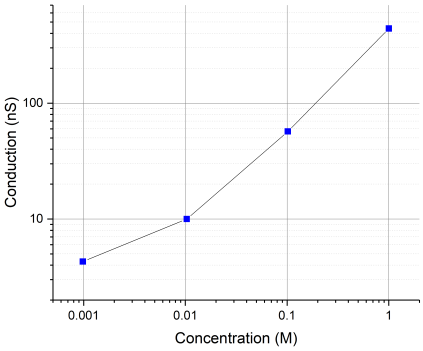

FIGURE 4.10: Conductance of a bare SiN nanopore ($\sim 70\,\text{nm}$) without graphene versus the concentration of KCl.

The following set of results follow from CV measurements at low salt concentration for 2 devices. CV measurements at 200 mV are run to determine the conductivity of the non-wetted system. The IV-curves are displayed in appendix L and from these measurements the conductances in table 4.3 are deduced. Though the concentration changes a factor 1000, the conductivity changes only a factor 10. Using equation 2.11, a typical Duhkin length at a graphene interface is 130 nm for 1 mM KCl and 0.13 nm for 1 M KCl. The expected defect size ranges from 0.5 nm to 2 nm[29]. Therefore, we predict that the conductivity of the nanopores in the graphene are dominated by the surface charge at low salt concentrations, explaining the little difference in conductivity between 1 mM and 1 M.

TABLE 4.3: Characterization of graphene-SiN devices at 200 mV for different salt concentrations.

Device	Conductance (nS) 1 mM	Conductance (nS) 1 M
6	1	15
7	0.6	14

The results for device 6 and 7 at respectively 1 V and 2.5 V are shown in figure 4.11 and 4.12. The IV-curves in figure 4.11 show a little electrowetting in the positive voltage domain. In general, the device shows a similar IV trend for both concentrations. The voltage window on device 7 is increased to 2.5 V, and enhanced current is observed at both concentrations as can be seen in figure 4.12. It is noteworthy that electrowetting at low concentration seems to happen at a higher potential. Furthermore, the hysteresis in the low salt system seems to be opposite compared to the 1 M system.

The change in relative conductivity between the graphene membrane and the bulk at low concentrations can dramatically alter the applied voltage required to start wetting. If the access resistance decreases by a factor of 1000 but the graphene resistance only decreases by a factor of 10, the voltage at the SiN Graphene interface will be significantly less for a given applied voltage. This means that a larger applied voltage is needed to overcome the threshold voltage for wetting at the interface. The result would be, as seen in figure 4.12, a shift in the voltage at which wetting starts away from the origin. This shift in the voltage has already been observed in the modeling results in figure 2.11c.

Another factor which might influence the system at low salt concentration is the EDL force. The Debye length at 1 mM KCl is ∼ 10 nm, compared to ∼ 0.3 nm at 1 M KCl. Therefore, electrostatics might come at play at lower salt concentrations.

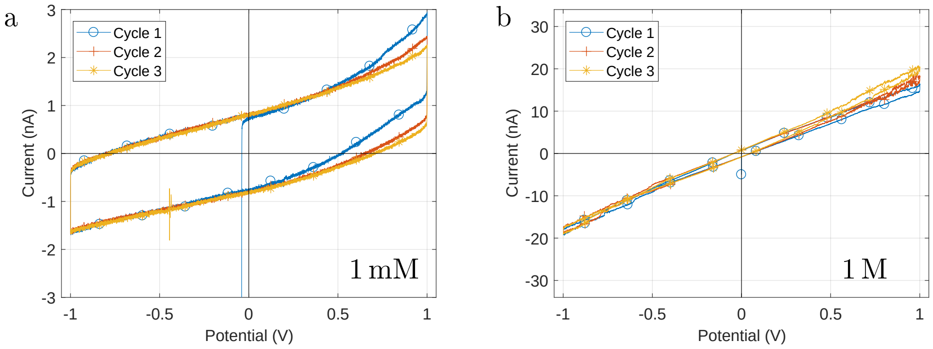

FIGURE 4.11: IV-curves of device 6 for different salt concentrations. The voltage is swept between $-1\,\mathrm{V}$ and $1\,\mathrm{V}$ with a scan rate of $10\,\mathrm{mVs}^{-1}$.

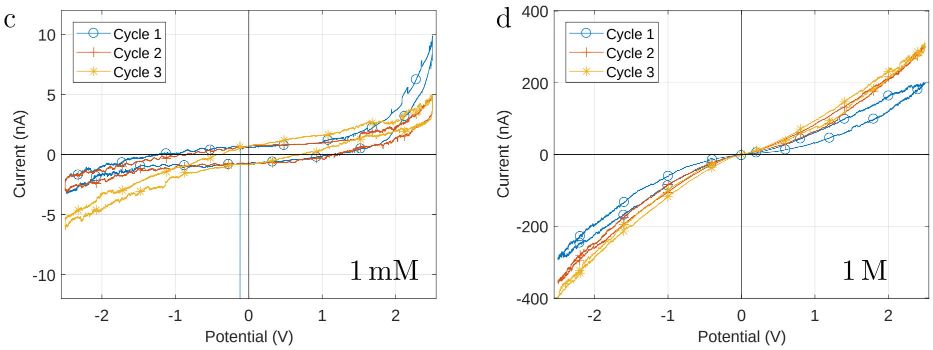

FIGURE 4.12: IV-curves of device 7 for different salt concentrations. The voltage is swept between $-2.5\,\mathrm{V}$ and $2.5\,\mathrm{V}$ with a scan rate of $10\,\mathrm{mVs}^{-1}$.

4.6 Pristine graphene

In this section some preliminary results with defect-less exfoliated graphene are discussed to raise some interesting questions for future work. The device uses a single flake of graphene placed on top of the SiN nanopore, as illustrated in figure 4.13a. One of the edges of the flake is placed intentionally very close to the pore. The first remark on the behavior of this device involves the very low conductivity of the system, which is obtained from figure 4.13b. Without electrowetting effects the conductivity is about 0.3 nS. This is in line with the fact that there are no ion transport enabling defects in the pristine graphene. The leak current can be caused by processes like proton transfer[47]. Electrowetting phenomena are observed in figure 4.13c. However, the magnitude of the current is much lower than for CVD graphene. Furthermore, the current shows oscillatory behavior. A possible explanation for this behavior is the electrowetting of the graphene till the closest edge. The graphene must detach to the closest edge of the graphene before a conduction channel can be formed. The moment the channel is formed, the new conductive path causes the voltage in the system to drop and the channel may close again if it drops too far. This cycle repeats and can account for the oscillatory behavior.

Preliminary experiments of optical reflection microscopy on the pristine graphene had unfortunately no success. The optical contrast was too low to observe any changes in the graphene-SiN interface.

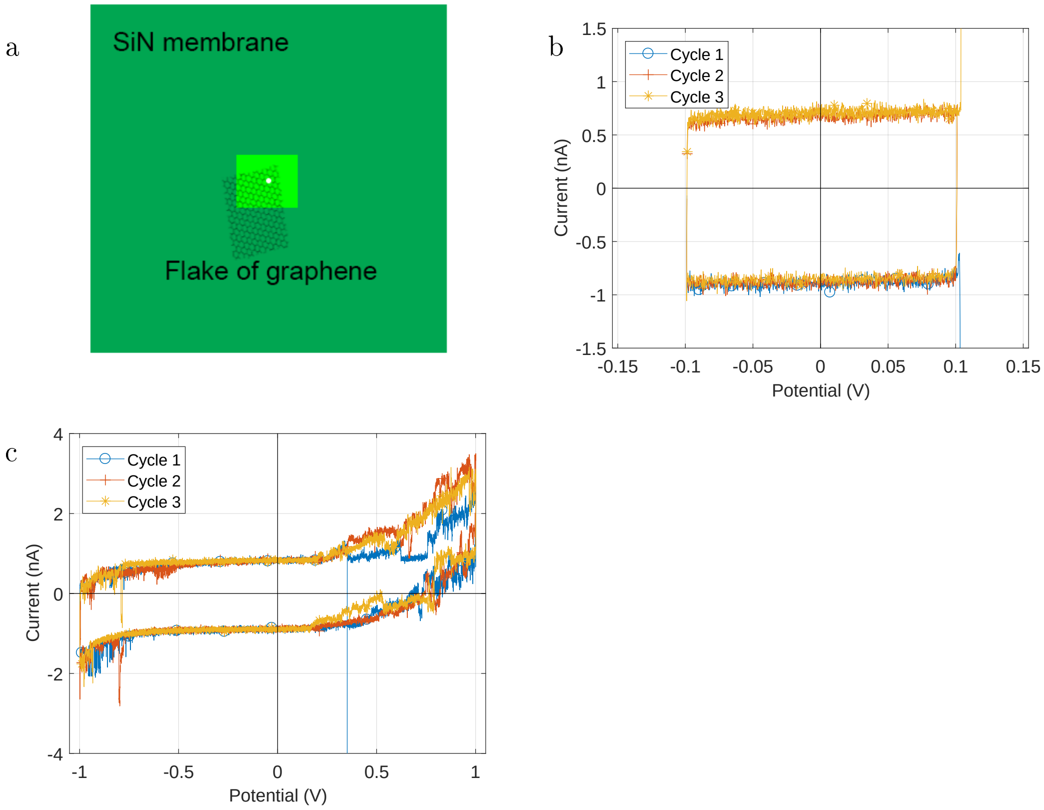

FIGURE 4.13: The device consists of a flake of pristine graphene (a). One of the edges is placed close to the SiN nanopore. The CV measurements are run from -100 to $100\,\mathrm{mV}$ (b) and -1 to $1\,\mathrm{V}$ (c) with a scan rate of $10\,\mathrm{mVs^{-1}}$.

Chapter 5

Conclusion and outlook

In this research multiple devices have been synthesized by suspending CVD graphene over a SiN nanopore to investigate the increased conductance of the system above a certain threshold voltage. So far, researchers have been troubled by the increased conductivity but the results were explained away as an artifact of deterioration of the graphene. The conducted experimental work presented here has shown that this increased conductivity is actually the result of electrowetting of the graphene-SiN interface, and is reversible in many cases.

In order to come to this conclusion, the quality of the monolayer graphene has been checked and a diversity of experimental methods have been used to characterize the devices. The electrochemical experiments have successfully enlarged the existing dataset and the optical and AFM measurements have confirmed the detachment of the graphene from the SiN substrate. Furthermore, a resistor model was developed to describe the basic IV-behavior of the system, confirming that electrowetting on its own can account for the observed conductivity.

The new electrochemical measurements have shown very rich IV-behavior with wide differences from device to device. Although the devices are strongly heterogeneous, the main underlying process of electrowetting is confirmed with the performed optical and AFM measurements. More detailed statements about the governing processes are hard to make, because of the heterogeneity of the devices and the still small dataset. However, a few interesting observations can be made, which are helpful for further testing. In general, the adhesion energy plays a dominant role in electrowetting and changes from device to device. This may be explained by the interplay of several factors. First of all, the roughness of the SiN substrate, the presence of wrinkles in the graphene and contaminations at the SiN substrate affects the adhesion energy. Furthermore, exposure of the SiN and graphene surface to the electrolyte solution for the first time after the first detachment may change the surface chemistry. The interplay of these factors becomes even more complicated when pH is introduced. pH has a large influence on the local surface chemistry, changing the interfacial capacitance, but this is out of the scope of this research.

The robustness of the IV-behavior around 0 V is poor. The graphene is likely to stay detached from the SiN substrate after multiple cycles. This may be explained by buckling of the graphene or contaminations at the graphene-SiN interface. The maximum height of the blister was estimated at 30 nm via the AFM measurements, which is much more, than the expected couple of Deybe lengths. This might point at other processes contributing to the inflation of the blister. In this case, the influence of electro-osmotic pressure (EOP) should be investigated.

To further improve the understanding of the system, more AFM measurements should be performed. This would not only give a larger dataset to test our theory, but AFM measurements at higher resolution would also improve the knowledge of the shape and size of the formed blister. Furthermore, additional measurements below the threshold voltage and at negative potential would contribute to extra understanding. Finally, a low salt concentration seemed to improve the robustness of the system, but more devices should be tested at these concentration to investigate this statement.

For current research it is valuable to keep in mind that the adhesion energy is of utmost importance to govern electrowetting. For future applications it would be valuable to have better control over electrowetting. This could enable applications like a predictable fluidic diode or ionic pumps and more.

Chapter 6

Acknowledgment

I would like to take this opportunity to acknowledge the assistance and contribution of a few people to this master thesis. First of all, I like to thank some people outside the BIOS group, who were so kind to spend time and effort on my research. Thanks to Eldad Grady from TU Eindhoven for his help and time with the graphene growth, Ine Segers-Nolten for the introduction to the Raman spectroscopy and Mark Smithers for the SEM measurements. I would like to thank Edwin Dollekamp and Harold Zandvliet of the Physics of Interfaces and Nanomaterials group for their close collaboration. Especially Edwin put a lot of time in the AFM measurements, which were very valuable for my research. Last but not least, I would like to thank Wesley van den Beld for the fruitful discussions and for transferring all his knowledge on the topic to me. I am grateful that I could continue the research based on your previous experiences and documentation.

I like to express my special gratitude to my supervisors for all their help and time. Thank you Josh, for making me so enthusiastic about this research. Working and discussing with you made my research really enjoyable. Vasilis, thank you for taking over the supervision when Josh left. I appreciated your curiosity on this topic. Jan, thank you for the weekly meetings, which always resulted in very useful discussions and new insights. Furthermore, I like to thank Hai and Johan for providing me with the right chips and Wouter for joining the examination committee.

Finally, I like to thank all the other BIOS members for the great time at BIOS. It is really nice working here!

Bibliography

[1] W. T. E. van den Beld, “Graphene and permalloy integration in functional fluidic and solid-state devices”, PhD thesis, Gildeprint, 2016.

[2] F Traversi, C Raillon, S. Benameur, K Liu, S Khlybov, M Tosun, D Krasnozhon, A Kis, and A Radenovic, “Detecting the translocation of dna through a nanopore using graphene nanoribbons”, *Nature nanotechnology*, vol. 8, no. 12, p. 939, 2013.

[3] S. Garaj, W Hubbard, A Reina, J Kong, D Branton, and J. Golovchenko, “Graphene as a subnanometre trans-electrode membrane”, *Nature*, vol. 467, no. 7312, p. 190, 2010.

[4] S. P. Surwade, S. N. Smirnov, I. V. Vlassiouk, R. R. Unocic, G. M. Veith, S. Dai, and S. M. Mahurin, “Water desalination using nanoporous single-layer graphene”, *Nature nanotechnology*, vol. 10, no. 5, pp. 459–464, 2015.

[5] A Gadaleta, C Sempere, S Gravelle, A Siria, R Fulcrand, C Ybert, and L Bocquet, “Sub-additive ionic transport across arrays of solid-state nanopores”, *Physics of Fluids*, vol. 26, no. 1, p. 012 005, 2014.

[6] H. Jussila, H. Yang, N. Granqvist, and Z. Sun, “Surface plasmon resonance for characterization of large-area atomic-layer graphene film”, *Optica*, vol. 3, no. 2, pp. 151–158, 2016.

[7] C. Lee, X. Wei, J. W. Kysar, and J. Hone, “Measurement of the elastic properties and intrinsic strength of monolayer graphene”, *science*, vol. 321, no. 5887, pp. 385–388, 2008.

[8] K. Sint, B. Wang, and P. Král, “Selective ion passage through functionalized graphene nanopores”, *Journal of the American Chemical Society*, vol. 130, no. 49, pp. 16 448–16 449, 2008.

[9] D. Cohen-Tanugi and J. C. Grossman, “Water desalination across nanoporous graphene”, *Nano letters*, vol. 12, no. 7, pp. 3602–3608, 2012.

[10] H. Qi, Z. Li, Y. Tao, W. Zhao, K. Lin, Z. Ni, C. Jin, Y. Zhang, K. Bi, and Y. Chen, “Fabrication of sub-nanometer pores on graphene membrane for ion selective transport”, *Nanoscale*, 2018.

[11] W. B. Russel, D. A. Saville, and W. R. Schowalter, *Colloidal dispersions*. Cambridge university press, 1989.

[12] J Sabio, C. Seoanez, S. Fratini, F Guinea, A. C. Neto, and F. Sols, “Electrostatic interactions between graphene layers and their environment”, *Physical Review B*, vol. 77, no. 19, p. 195 409, 2008.

[13] W. Gao and R. Huang, “Effect of surface roughness on adhesion of graphene membranes”, *Journal of Physics D: Applied Physics*, vol. 44, no. 45, p. 452 001, 2011.

[14] H Gerischer, “An interpretation of the double layer capacity of graphite electrodes in relation to the density of states at the fermi level”, *The Journal of Physical Chemistry*, vol. 89, no. 20, pp. 4249–4251, 1985.

[15] M. D. Stoller, C. W. Magnuson, Y. Zhu, S. Murali, J. W. Suk, R. Piner, and R. S. Ruoff, "Interfacial capacitance of single layer graphene", *Energy & Environmental Science*, vol. 4, no. 11, pp. 4685–4689, 2011.

[16] H. Ji, X. Zhao, Z. Qiao, J. Jung, Y. Zhu, Y. Lu, L. L. Zhang, A. H. MacDonald, and R. S. Ruoff, "Capacitance of carbon-based electrical double-layer capacitors", *Nature communications*, vol. 5, p. 3317, 2014.

[17] T. Fang, A. Konar, H. Xing, and D. Jena, "Carrier statistics and quantum capacitance of graphene sheets and ribbons", *Applied Physics Letters*, vol. 91, no. 9, p. 092 109, 2007.

[18] J. Xia, F. Chen, J. Li, and N. Tao, "Measurement of the quantum capacitance of graphene", *Nature nanotechnology*, vol. 4, no. 8, p. 505, 2009.

[19] P. A. Brooksby, A. K. Farquhar, H. M. Dykstra, M. R. Waterland, and A. J. Downard, "Quantum capacitance of aryldiazonium modified large area few-layer graphene electrodes", *The Journal of Physical Chemistry C*, vol. 119, no. 46, pp. 25 778–25 785, 2015.

[20] J.-H. Zhong, J.-Y. Liu, Q. Li, M.-G. Li, Z.-C. Zeng, S. Hu, D.-Y. Wu, W. Cai, and B. Ren, "Interfacial capacitance of graphene: Correlated differential capacitance and in situ electrochemical raman spectroscopy study", *Electrochimica Acta*, vol. 110, pp. 754–761, 2013.

[21] E. J. Santos and E. Kaxiras, "Electric-field dependence of the effective dielectric constant in graphene", *Nano letters*, vol. 13, no. 3, pp. 898–902, 2013.

[22] R. Van Hal, J. C. Eijkel, and P. Bergveld, "A general model to describe the electrostatic potential at electrolyte oxide interfaces", *Advances in colloid and interface science*, vol. 69, no. 1-3, pp. 31–62, 1996.

[23] B. J. Kirby, *Micro-and nanoscale fluid mechanics: transport in microfluidic devices*. Cambridge University Press, 2010.

[24] F. Mugele and J.-C. Baret, "Electrowetting: From basics to applications", *Journal of Physics: Condensed Matter*, vol. 17, no. 28, R705, 2005.

[25] W. Gao, P. Xiao, G. Henkelman, K. M. Liechti, and R. Huang, "Interfacial adhesion between graphene and silicon dioxide by density functional theory with van der waals corrections", *Journal of Physics D: Applied Physics*, vol. 47, no. 25, p. 255 301, 2014.

[26] S. P. Koenig, N. G. Boddeti, M. L. Dunn, and J. S. Bunch, "Ultrastrong adhesion of graphene membranes", *Nature nanotechnology*, vol. 6, no. 9, p. 543, 2011.

[27] R. R. Thomas, F. B. Kaufman, J. T. Kirleis, and R. A. Belsky, "Wettability of polished silicon oxide surfaces", *Journal of The Electrochemical Society*, vol. 143, no. 2, pp. 643–648, 1996.

[28] S. Wang, Y. Zhang, N. Abidi, and L. Cabrales, "Wettability and surface free energy of graphene films", *Langmuir*, vol. 25, no. 18, pp. 11 078–11 081, 2009.

[29] T. Jain, B. C. Rasera, R. J. S. Guerrero, M. S. Boutilier, S. C. O'hern, J.-C. Idrobo, and R. Karnik, "Heterogeneous sub-continuum ionic transport in statistically isolated graphene nanopores", *Nature nanotechnology*, vol. 10, no. 12, p. 1053, 2015.

[30] M. S. Boutilier, C. Sun, S. C. O'Hern, H. Au, N. G. Hadjiconstantinou, and R. Karnik, "Implications of permeation through intrinsic defects in graphene on the design of defect-tolerant membranes for gas separation", *Acs Nano*, vol. 8, no. 1, pp. 841–849, 2014.

[31] A. C. Ferrari, J. Meyer, V Scardaci, C Casiraghi, M. Lazzeri, F. Mauri, S Piscanec, D. Jiang, K. Novoselov, S Roth, *et al.*, “Raman spectrum of graphene and graphene layers”, *Physical review letters*, vol. 97, no. 18, p. 187 401, 2006.

[32] L. Malard, M. Pimenta, G Dresselhaus, and M. Dresselhaus, “Raman spectroscopy in graphene”, *Physics Reports*, vol. 473, no. 5-6, pp. 51–87, 2009.

[33] F Tuinstra and J. L. Koenig, “Raman spectrum of graphite”, *The Journal of Chemical Physics*, vol. 53, no. 3, pp. 1126–1130, 1970.

[34] R. R. Nair, P. Blake, A. N. Grigorenko, K. S. Novoselov, T. J. Booth, T. Stauber, N. M. Peres, and A. K. Geim, “Fine structure constant defines visual transparency of graphene”, *Science*, vol. 320, no. 5881, pp. 1308–1308, 2008.

[35] D. Lide, *CRC Handbook of Chemistry and Physics*. CRC Press, 2003.

[36] M. E. Suk and N. Aluru, “Ion transport in sub-5-nm graphene nanopores”, *The Journal of chemical physics*, vol. 140, no. 8, p. 084 707, 2014.

[37] I Vodyanoy and S. Bezrukov, “Sizing of an ion pore by access resistance measurements”, *Biophysical journal*, vol. 62, no. 1, p. 10, 1992.

[38] J. E. Hall, “Access resistance of a small circular pore.”, *The Journal of general physiology*, vol. 66, no. 4, pp. 531–532, 1975.

[39] C. Lee, L. Joly, A. Siria, A.-L. Biance, R. Fulcrand, and L. Bocquet, “Large apparent electric size of solid-state nanopores due to spatially extended surface conduction”, *Nano letters*, vol. 12, no. 8, pp. 4037–4044, 2012.

[40] L. Bocquet and E. Charlaix, “Nanofluidics, from bulk to interfaces”, *Chemical Society Reviews*, vol. 39, no. 3, pp. 1073–1095, 2010.

[41] X. Li, W. Cai, J. An, S. Kim, J. Nah, D. Yang, R. Piner, A. Velamakanni, I. Jung, E. Tutuc, *et al.*, “Large-area synthesis of high-quality and uniform graphene films on copper foils”, *Science*, vol. 324, no. 5932, pp. 1312–1314, 2009.

[42] S. Bhaviripudi, X. Jia, M. S. Dresselhaus, and J. Kong, “Role of kinetic factors in chemical vapor deposition synthesis of uniform large area graphene using copper catalyst”, *Nano letters*, vol. 10, no. 10, pp. 4128–4133, 2010.

[43] E. Dollekamp, P. Bampoulis, B. Poelsema, H. J. W. Zandvliet, and E. S. Kooij, “Electrochemically induced nanobubbles between graphene and mica”, *Langmuir*, vol. 32, no. 26, pp. 6582–6590, 2016.

[44] Y. Zhang, T. Gao, Y. Gao, S. Xie, Q. Ji, K. Yan, H. Peng, and Z. Liu, “Defect-like structures of graphene on copper foils for strain relief investigated by high-resolution scanning tunneling microscopy”, *ACS nano*, vol. 5, no. 5, pp. 4014–4022, 2011.

[45] W. Zhu, T. Low, V. Perebeinos, A. A. Bol, Y. Zhu, H. Yan, J. Tersoff, and P. Avouris, “Structure and electronic transport in graphene wrinkles”, *Nano letters*, vol. 12, no. 7, pp. 3431–3436, 2012.

[46] Y. Zhang, N. Wei, J. Zhao, Y. Gong, and T. Rabczuk, “Quasi-analytical solution for the stable system of the multi-layer folded graphene wrinkles”, *Journal of Applied Physics*, vol. 114, no. 6, p. 063 511, 2013.

[47] S Hu, M Lozada-Hidalgo, F. Wang, A Mishchenko, F Schedin, R. Nair, E. Hill, D. Boukhvalov, M. Katsnelson, R. Dryfe, *et al.*, “Proton transport through one-atom-thick crystals”, *Nature*, vol. 516, no. 7530, p. 227, 2014.

[48] L. Bousse and S. Mostarshed, “The zeta potential of silicon nitride thin films”, *Journal of electroanalytical chemistry and interfacial electrochemistry*, vol. 302, no. 1-2, pp. 269–274, 1991.

[49] Y. Rao, *Heat Transfer*. Universities Press, 2001.

Appendix A

Electro-osmotic flow and pressure

The combination of potential differences and EDLs in the system might lead to electro-osmitic flow (EOF) and electro-osmitic pressure (EOP). The magnitude and therefore the importance of these phenomena will be examined in the next paragraphs.

At low potential the graphene is expected to fully cover the nanopore in the substrate without wetting effects. Defects in the graphene directly on top of the nanopore will result in a small current through the system. Neglecting the small current, this situation can be approximated by a closed cylinder with zero net flow rate $Q_{\mathrm{tot}} = 0$ and a pressure gradient of Δp. [23] The potential difference ΔV is applied over a cylindrical nanopore of length L and radius r, resulting in equation A.1 [23] using a thin-EDL limit.

$$\frac{\Delta p}{\Delta V} = -\frac{8\mu_{\mathrm{EO}}\eta}{r^2} \tag{A.1}$$

$$\tag{A.2}$$

with μ_{EO} the electro-osmotic mobility and η the dynamic viscosity. The dynamic viscosity $\eta = 1 \times 10^{-3}\,\mathrm{Pa\,s}$[23]. The electro-osmotic mobility as given in equation A.3 can be used for simple interfaces in fluids with uniform properties. [23]

$$\mu_{\mathrm{EO}} = -\frac{\epsilon\zeta}{\eta} \tag{A.3}$$

with ϵ the electric permittivity and ζ the zeta potential.

In a system with a silicon nitride interface $\zeta = -30\,\mathrm{mV}$ [48] and $\epsilon = 6 \times 10^{-11}\,\mathrm{Fm^{-1}}$, resulting in an electro-osmotic mobility of $\mu_{\mathrm{EO}} = 2 \times 10^{-9}\,\mathrm{m^2V^{-1}s^{-1}}$.

Assuming an potential of 1 V is applied over the cylinder with dimensions $r = 25 \times 10^{-9}\,\mathrm{m}$ and $L = 40 \times 10^{-9}\,\mathrm{m}$. Most of the potential drop will be over the graphene and a little over the pore. This results in a pressure difference of $\Delta p = -0.6\,\mathrm{kPa}$. The energy relating this pressure is the pressure drop times the volume $E_{\mathrm{p}} = \Delta p \pi r^2 L = 5 \times 10^{-20}\,\mathrm{J}$. The energy in a closed system resulting from the interfacial energy is dependent on the specific capacitance of graphene $C_{\mathrm{gr}} = 0.08\,\mathrm{Fm^{-2}}$[20]. The interfacial energy for the exposed graphene of area πr^2 is $\frac{1}{2}C_{\mathrm{gr}}\pi r^2\phi^2 = 7 \times 10^{-17}\,\mathrm{J}$. Therefore, the energy resulting from the pressure is negligible.

EOF in the blister The influence of the EOF in the blister should be investigated in the future. A few assumptions can be made to come to a result: $\bar{v}_{\mathrm{p}} = \Delta p \frac{h^2}{12\mu}$ (flat plate flow) and $\bar{v}_{\mathrm{EOF}} = \frac{\boldsymbol{E}\epsilon\zeta}{\mu}$ ($\boldsymbol{E}$ vector field from resistor model) are equal. Solving this expression and integrating the pressure over the area gives a force/energy on the graphene.

Appendix B

Annular resistance

The derivation for the annular resistance is based on a classical heat transfer problem: heat conduction through a hollow cylinder[49].

$$I = -\kappa A \frac{dV}{dr} \tag{B.1}$$

$$\int_{r_1}^{r_2} \frac{I}{A} dr = -\int_{V_1}^{V_2} \kappa dV \tag{B.2}$$

$$\int_{r_1}^{r_2} \frac{I}{2\pi r h} dr = -\int_{V_1}^{V_2} \kappa dV \tag{B.3}$$

$$\frac{I}{2\pi r h \kappa} \ln(\frac{r_{n+1}}{r_n}) = \Delta V \tag{B.4}$$

$$R_\mathrm{s}(r_n) = \frac{\Delta V}{I} = \frac{1}{\kappa 2\pi h} \ln(\frac{r_{n+1}}{r_n}) \tag{B.5}$$

with the conductivity κ, the area A, the inner voltage V_1, the outer voltage V_2, the blister height h and r_n the radius of the blister, which is incremented by dr.

Appendix C

MATLAB code resistor model

```
clc
clear all

Vmax = 1;                 %Max voltage [V]
Vtres = 0.2;              %Threshold voltage [V]
kappa = 11;               %Bulk conductivity [1/(Ohm*m)]
h = 10E-9;                %Blister height [m]
R0 = 122E6;               %Initial resistance no wetting [Ohm]
r_ini = 27E-9;            %Initial pore size [m]
spacing = 70E-9;          %Defect spacing
d0 = 200E6;               %Defect resistance
Rac = 3E6;                %Access resistance SiN pore [Ohm]
dr = 1E-9;                %Stepsize r [m]

nabla_s = 1./(2*pi*kappa*h);     %Sheet resistivity Rs [Ohm m]
nabla_p = d0*spacing.^2;         %Graphene Resistivity Rp [Ohm
    m^2]

K = 1000;                 %# of voltage iterations
Vin = 0:Vmax/K:Vmax;

f = figure
for k = 1:1

    State_n = 1; %first state, zero expansions
    for i = 1:1:K+1 %find network for all given voltages
        [Rs,Rp,n(:,i),Vn(1:n(:,i)+3,i),dR(k,i),State_n] =
            Rnet(Vin(1,i), Vtres, nabla_s, nabla_p, R0, dr,
            Rac, State_n, r_ini);
    end
    %Calc total current in the system through Raccess
    I(:,k) = (Vn(2,:)-Vn(3,:))/Rac;

end

%Plot IV-curve
f = figure
plot(Vin,I*1E9)
hold on
set(gca,'fontsize',14)
```

```
xlabel('V_{in}(V)','FontSize',14)
ylabel('I(nA)','FontSize',14)
grid on

%Plot blister diameter
f = figure
plot(Vin,2*dR*1E9)
set(gca,'fontsize',14)
xlabel('V_{in}(V)','FontSize',14)
ylabel('Blister diameter (nm)','FontSize',14)
grid on

%% Equivalent resistance of blister

Req = (Vin'-I(:,k)*Rac)./I(:,k);

%plot V0 and Req
yyaxis right
plot(Vin,Vn(3,:))
set(gca,'fontsize',14)
xlabel('V_{in}(V)','FontSize',14)
ylabel('V_0 (V)','FontSize',14)

yyaxis left
plot(Vin,Req/1E6)
set(gca,'fontsize',14)
xlabel('V_{in}(V)','FontSize',14)
ylabel('R_{eq} (M\Omega)','FontSize',14)
grid on
```

```
function [Rs,Rp,nr,Vn,dR,State_n] = Rnet(Vin, Vtres, nabla_s,
    nabla_p, R0, dr, Rac, State_n, r_ini)
%Rnet(Vin, Vtres, nabla_s, nabla_p, R0, dr, Rac, State_n,
   r_ini)
%Vin          Input voltage
%Vtres        Threshold voltage
%Nabla        Resistivity
%R0           Initial resistance
%dr           Stepsize
%Rac          Access resistance
%State_n      Previous state
%r_ini        Initial radius system

if State_n == 0
    State_n = 1;
end

ground = 1; %Ground node
Vn_stable = [0;Vin;Vin*R0/(Rac+R0)];

for n = 1:State_n
```

```
    %Initialization of R and NetList
    Rs(n) = Rseries(nabla_s, dr, n, r_ini);
    Rp(n) = Rparallel(nabla_p, dr, n, r_ini);
    NetList(1,:) = [2 3 Rac];
    NetList(2,:) = [3 ground R0];
    NetList(2*n+1,:) = [n+2 n+3 Rs(n)];
    NetList(2*n+2,:) = [n+3 ground Rp(n)];
end

expand = 1;
while expand == 1

    %Calculate resistance for new dr
    Rs(n) = Rseries(nabla_s, dr, n, r_ini);
    Rp(n) = Rparallel(nabla_p, dr, n, r_ini);

    %Expand NetList
    NetList(1,:) = [2 3 Rac];
    NetList(2,:) = [3 ground R0];
    NetList(2*n+1,:) = [n+2 n+3 Rs(n)];
    NetList(2*n+2,:) = [n+3 ground Rp(n)];

    Vnod=[2 Vin; ground 0];

    l=size(NetList,1);
    N=max([NetList(:,1) ;
        NetList(:,2)]);
    A=zeros(N,N);
    B=zeros(N,1);

    for i=1:l
        n1=NetList(i,1);
        n2=NetList(i,2);
        if n1==n2
        else
            A(n1,n2)=A(n1,n2)-1/NetList(i,3);
            A(n2,n1)=A(n2,n1)-1/NetList(i,3);
            A(n1,n1)=A(n1,n1)+1/NetList(i,3);
            A(n2,n2)=A(n2,n2)+1/NetList(i,3);
        end
    end
    for i=1:size(Vnod,1)
        A(Vnod(i,1),:)=zeros(1,N);
        A(Vnod(i,1),Vnod(i,1))=1;
        B(Vnod(i,1),1)=Vnod(i,2);
    end

    %Calculate voltage nodes of the system
    Vn = A\B;
    %Check if last node is below Vtres
    if Vn(end,1) < Vtres
```

```
        %stop expansion
        expand = 0;
        nr = n-1;
        dR = nr*dr;
        Vn = Vn_stable; %Previous state is the stable system
        State_n = n-1;
        X = sprintf('Vin = %f',Vn(i,1));
        disp(X);
    end
    %Save state
    Vn_stable = Vn;
    n = n+1;
end
end
```

```
function [ Rs ] = Rseries( nabla_s, dr, n, r_ini)
%Calculation of Rs
%   nabla_s     conduction
%   dr          stepsize radius
%   n           number of extentions
%   r_ini       inner radius

Rs = nabla_s*log(((n+1)*dr+r_ini)/(n*dr+r_ini));

end
```

```
function [ Rp ] = Rparallel( nabla_p, dr, n, r_ini)
%Calculation of Rs
%   nabla_p     conduction
%   dr          stepsize radius
%   n           number of extentions
%   roff        inner radius

Rp = nabla_p/(pi*((r_ini+(n+1)*dr)^2-(r_ini+n*dr)^2));

end
```

Appendix D

Transmittance measurements

Contrary to the local Raman measurements, another method, can be used to determine the number of grown graphene layers over a larger area. As explained in section 2.2.2 the level of transmittance is a measure for the number of graphene layers. Unfortunately, the transmittance is not merely affected by the graphene layers, but also by the SiN membrane. The transmittance of different chips will vary, due to differences in the thickness of the SiN membrane. In figure D.1 a thickness profile is given for a SiN membrane, which varies between 38.8 nm to 40.2 nm. To obtain a reliable result there will be compensated for the variation of SiN thickness between different chips. The coefficient A is introduced to fit the transmittance $T(\omega)$ of a graphene chip to a reference chip without graphene $T(\omega)_{reference}$. (This needs more explanation!) A linear relation follows:

$$T(\omega) = AT(\omega)_{reference} + G \tag{D.1}$$

with A the correction coefficient for the SiN thickness, $T(\omega)_{reference}$ and G an absorption factor due to N layers of graphene. Both constants A and G can be determined by fitting a linear line in the measured relation of $T(\omega)$ versus $T(\omega)_{reference}$.

Measurements are done using an Ocean Optic HR400 spectrometer with a wavelength range of 200 nm to 1100 nm and a Leica DM6000 M microscope with a 12V 100 W halogen lamp. The integration time is set to 100 ms and 20 samples are averaged. Furthermore, the obtained spectra are post-processed with a moving average filter and corrected for the changes in SiN membrane thickness using the given relation in equation D.1).

The tranmittance measurements are shown in figure D.2. Using equation 2.7 with $f(\omega)$ of 1.13 at 550 nm the transmittance should be about 97.5% [34].

To sum up, the transmittance measurements are not as reliable as hoped for, due to the significant variations in membrane thickness between different chips. In the future the reference measurement and the measurement with the graphene must be done on the same SiN membrane to get a reliable result.

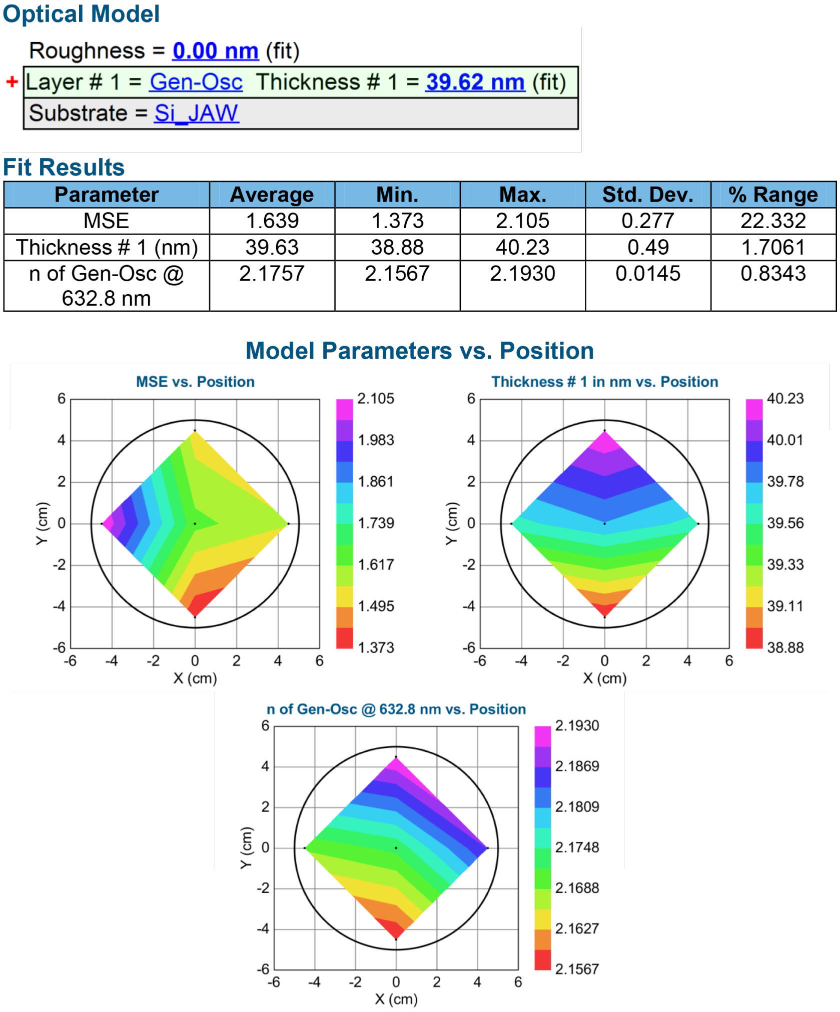

Optical Model

Roughness = **0.00 nm** (fit)

+ Layer # 1 = Gen-Osc Thickness # 1 = **39.62 nm** (fit)

Substrate = Si_JAW

Fit Results

Parameter	Average	Min.	Max.	Std. Dev.	% Range
MSE	1.639	1.373	2.105	0.277	22.332
Thickness # 1 (nm)	39.63	38.88	40.23	0.49	1.7061
n of Gen-Osc @ 632.8 nm	2.1757	2.1567	2.1930	0.0145	0.8343

Model Parameters vs. Position

FIGURE D.1: Measurements on the membrane thickness of a SiN membrane.

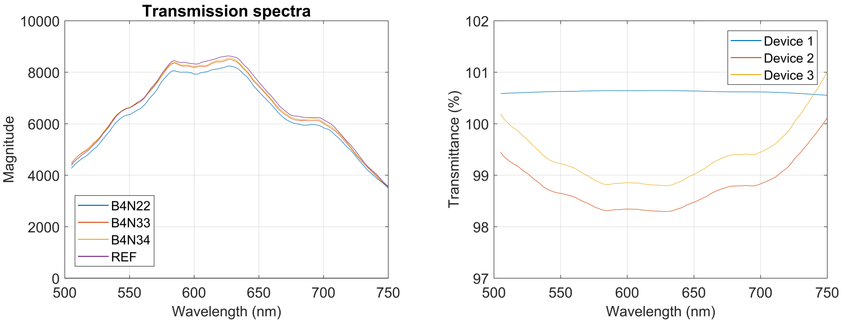

FIGURE D.2: The left figure shows the optical spectrum for all tested devices and the reference spectrum. The right figure indicates the transmittance of the graphene devices relative to the reference spectrum.

Appendix E

Graphene grow protocol

Monolayer graphene is grown in collaboration with E. Grady at the Plasma & Materials Processing (PMP) department of Eindhoven University of Technology. The graphene is synthesized on copper by means of low pressure chemical vapor deposition (LPCVD) in the CVD system shown in figure E.1. The described graphene synthesize is based on the previous work and expertise of W. van den Beld and E. Grady[1].

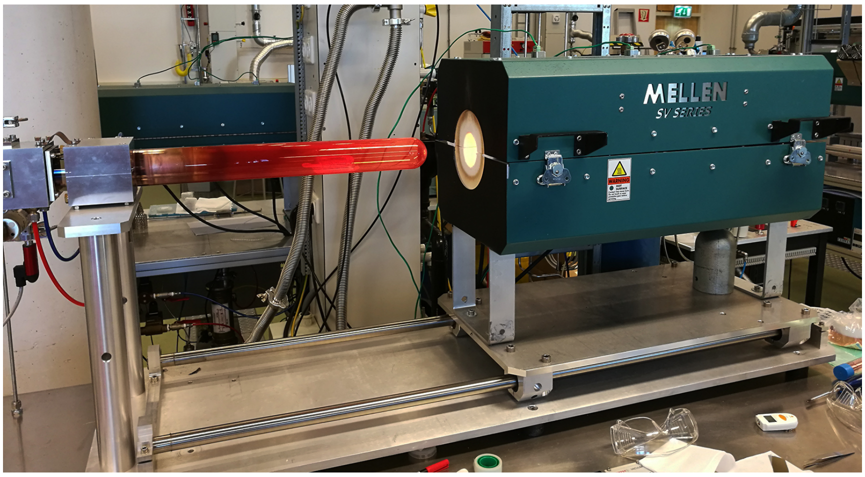

FIGURE E.1: The setup shows the CVD system of the PMP department at the Eindhoven University of Technology a few seconds after the quartz tube is removed from the furnace. The quartz tube on the left contains a quartz boat onto which the copper foil is loaded. The furnace on the right can be slide onto the tube.

99.8% Alfa Aesar no. 13382 (coated by a thin film of chromium oxide) copper foil is used as catalyst. Prior to the synthesize, the copper sheets are cleaned. The cleaning steps are subsequently: acetone for 30 min, methanol for 1 min and finally for 30 s in 1 M nitric acid.

In the meantime the furnace is heated to 1050 °C and the quartz tube is purged with argon gas. Thereafter, the tube is pumped down to $\sim 5 \times 10^{-3}$ mbar. Next, the furnace is moved over the quartz tube and the copper is annealed for 45 min at 1050 °C with a hydrogen flow of 10 sccm and an argon flow of 500 sccm. Lastly, the graphene is grown for 20 min at 1050 °C with an additional methane flow of 100 sccm, a reduced hydrogen flow of 6 sccm and the same argon flow of 500 sccm.

Appendix F

Raman spectra

An area of 10x10 µm^2 is scanned with 9 measurement points. The used Raman setup consists of a WITec Alpha 300 system. The Raman spectra are recorded using a 532 nm (2.33 eV) laser at 1 mW using a 100x objective ($NA = 0.9$) and 2 s integration time. The spot size of each measurement is $\frac{1.22\Lambda}{NA} = 0.72$ µm with Λ the wavelength and NA the numerical aperture. A flake of graphene is transferred to a silicon substrate with a 300 nm thick silicon dioxide layer.

The Raman spectra are processed with a MATLAB script. The processing involves determining the offset in the spectrometer by fitting the Rayleigh peak and Lorentzian curves are fitted to obtain the position and intensity of the graphene peaks[1]. The resulting Raman spectra are shown below in figure F.1.

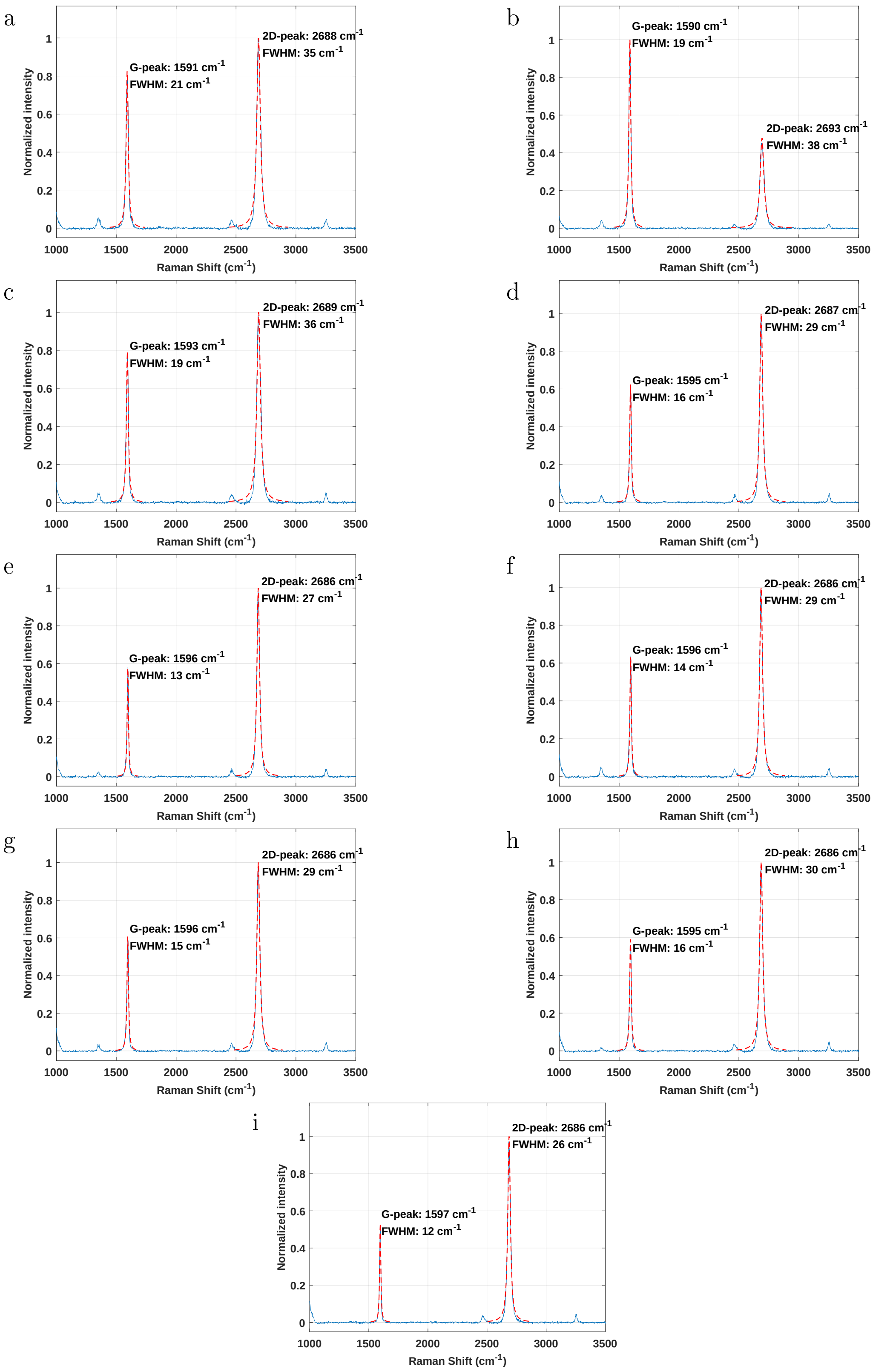

FIGURE F.1: Raman spectra of 9 measurement points in a scanned area of 10x10 µm^2.

Appendix G

SiN membrane characterization

The graphene is transferred to a 16.15x16.15 mm silicon chip with a $\sim$ 40 nm thick silicon nitride (SiN) membrane on top. The silicon chip is back etched, such that a 80x80 µm SiN membrane is left over in the middle of the chip. The membrane contains an ion laser beamed hole of approximately 50 nm as is shown in figure G.1. The aspect ratio's of the pore's in different SiN membranes are depicted in table G.1. The position of the ion beamed hole can deviates several tens of nanometers from the membrane's center. The fabrication process of the SiN membranes is described in the work of van den Beld[1].

An overview of all SiN membranes is given in table G.1. The conductance of each bare pore is determined by means of CV. The CV measurements are run from -200 mV to 200 mV for 3 cycles with a scan rate of 10 mVs^{-1}. The measurements are performed in the closed holder with SCEs connected to the Bio-Logic VSP potentiostat. The resulting IV-curve of each chip is shown in figure G.2 and G.3.

Table G.1: Characterization table of SiN membranes.

Chip	Pore Size (µm)		Conductance (nS)	Status
	a	b	1M KCl	
N14	43	43	~2	Bad
N21	50	50	~75	Good
N22	47	67	~100	Good
N23	49	65	~250	Good
N24	48	51	~40	Bad
N31	29	75	~10	Bad
N32	72	152	~15	Bad
N33	53	57	~175	Good
N34	50	50	~175	Good
N41	52	52	~150	Good
N42	54	54	~200	Good
N43	50	50	~125	Good
N44	42	42	~200	Good

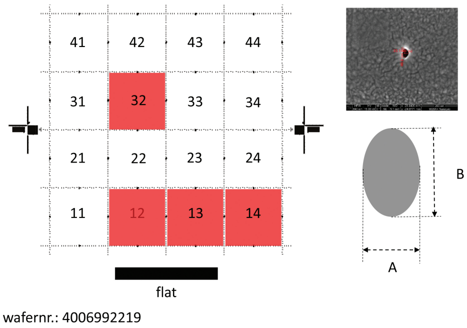

FIGURE G.1: Overview of all silicon nitride chips and the aspect ratios of the ion beamed hole per chip.

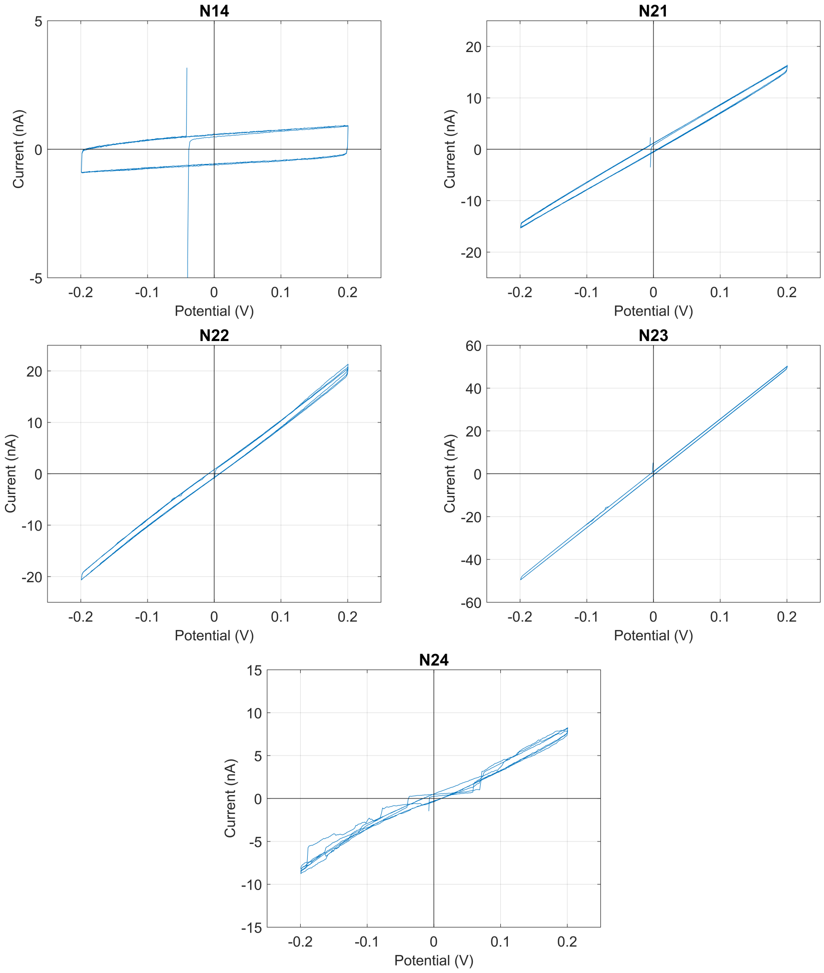

FIGURE G.2: Conductivity measurements for all bare silicon nitride chips.

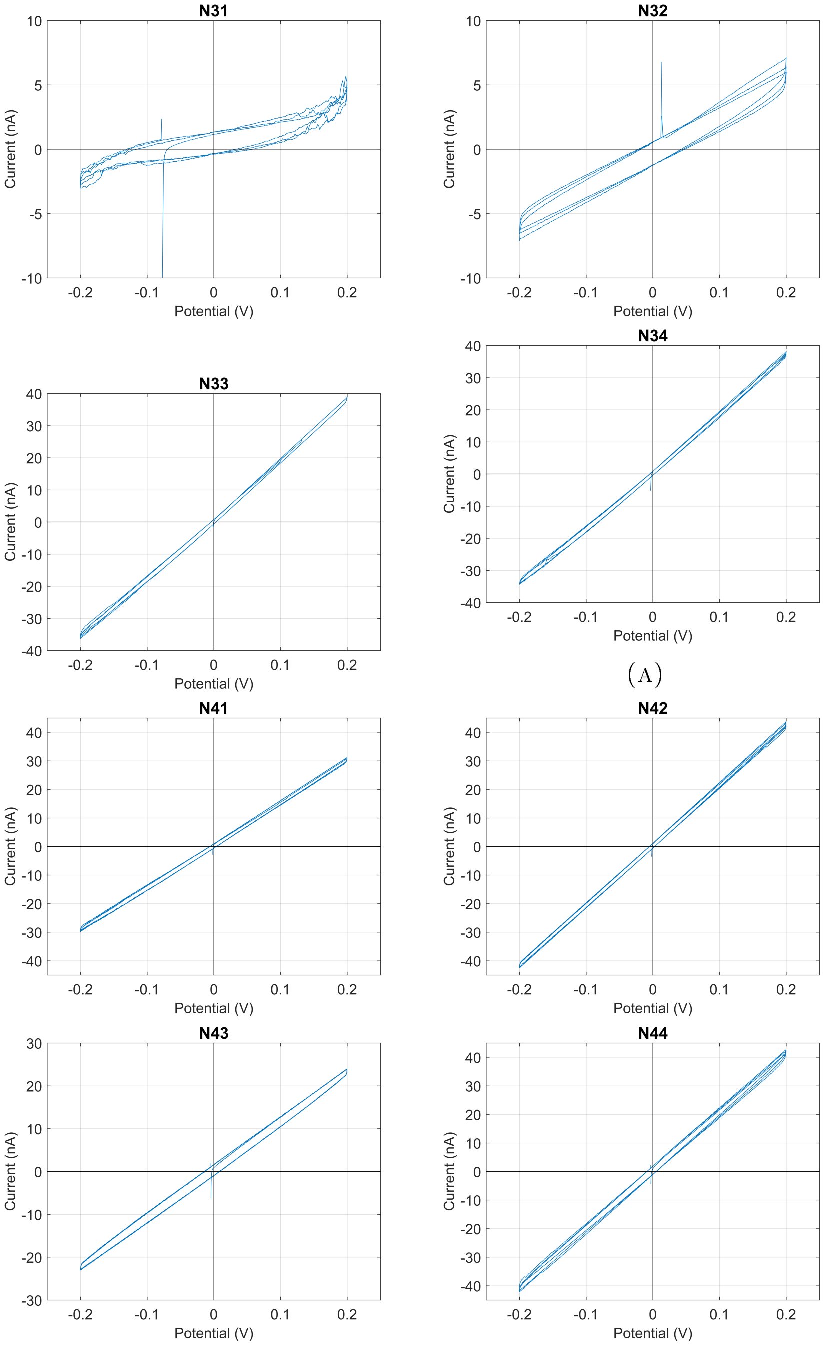

(A)

FIGURE G.3: Conductivity measurements for all bare silicon nitride chips continued.

Appendix H

Graphene transfer protocol

The used transfer protocol is shown below.

Graphene transfer V4

Douwe de Bruijn – BIOS – tel: 0630740611

CVD grown graphene on copper will be transferred to a SiN or SiO_2 substrate using PMMA.

Batch number: _______
Date: _______________
Copper ID: __________________, grown in ________________________
Stored at: ____

0. Process overview

Process step	Date	Time	Remarks
Spin coating PMMA			~1.5 hours
Cutting			~30 min
Removing backside graphene			~30 min
Etching copper			~10 hours
Rinsing, scooping and post-baking			Cleaning: ~2-3 hours Post-baking: >2 hours
Measuring			
Dissolving PMMA			~1.5 hours
Characterization			

1. Spin coating PMMA

PMMA is spin coated on top of the graphene and subsequently pre-baked. The PMMA layer should be thick enough to give enough support later on in the process. Cover all edges of the graphene with tape when taping the graphene on a wafer to prevent PMMA from leaking underneath the sample. Furthermore, use the backside of the graphene sample.

Date: ________________
_______ µl (*1 ml*) of PMMA from batch _____________________
Spin coat settings: ______ rpm (*2200 rpm*) for ______ sec (*30 sec*) at _____ rpm/sec (*500 rpm/sec*)*
Dried at _____ °C (RT) for _____ min (*>30 min*)
Pre-baked at____ °C (*125 °C*) for _____ min (*30 min*)

The graphene should be stored as follows. Take an air tide box and put some orange desiccant beads in the box. Pump down air and introduce N_2. Do this multiple times.

Notes: ____

* Layer of ~100 nm for PMMA A2 (Anisole 2%)

2. Cutting

Cutting of the graphene on copper. Make sure you only use pitching movements to prevent shear stress on the graphene.

Date: ________________

Graphene cut into _____ pieces using ___________________

Sample	Size (~mm x mm)	Notes
1.	*5 x 5*	
2.		
3.		
4.		

Notes: ____

3. Removing backside graphene with nitric acid

Removing the backside graphene layer with ~4 M HNO_3. Make sure all HNO_3 is removed from the sample before continuing to the next step!

Date: ________________

____ ml (*2 ml*) HNO_3 (69%) mixed with _____ ml (*6 ml*) DI water in a watch glass.

Etching time: ____ sec (*1 min*) in HNO_3. Subsequently submerge ____ times (*2 times*) for ____ sec (10 *sec*) in MilliQ water and rinse for _______ sec (*>2 min*) in MilliQ water.

Notes: ____

4. Etching copper

Etching copper with low concentrated APS (~40 mM), thereafter rising the sample in a DI water vortex and afterwards drying the sample.

Date: ________________

a. Etching
   Amount of APS: _____ g (1 wt%)
   Amount of DI water: ______ g
   Etching time: ______ hour (*8-9 hours*)

Notes: ____

5. Rinsing, scooping and post-baking

Thoroughly cleaning the SiN or SiO_2 chips and cleaning the graphene samples in a DI water vortex. Where after the graphene is scooped on the chips and post-baked (overnight).

Date: ________________

a. Cleaning the chips:
    a. New chips:
    Piranha >80 °C (15 min) -> 3x DI -> Acetone (10 min) -> Ethanol (2 min) -> 3x DI -> Spin dry -> O_2 plasma (30 min) -> Milliq water
    b. Reusing chips:
    HNO_3 80 °C (15 min) -> DI -> RCA-2 80 °C (15 min) -> 3x DI -> Piranha >80 °C (15 min) -> 3x DI water -> Acetone (10 min) -> Ethanol (2 min) -> 3x DI water -> Spin dry -> O_2 plasma (30 min) -> DI water
b. Rinsing the graphene/PMMA samples in a DI water vortex until the conductivity of the drainage water stabilizes.
b. Scooping the graphene with the PMMA on the cleaned chip.
c. Post-baking the sample at 125 °C for at least 2 hours (overnight is even better) to form the PMMA to the substrate.

Sample	**Last conductivity (µS/cm)**	**Substrate (SiN/SiO_2)**	**Post-bake T (°C)** *(125 °C)*	**Time (min)** *(> 2 hour)*	**Notes on scooping**
1.					
2.					
3.					
4.					
5.					
6.					

Notes: ____

6. Measuring

Visual check if samples are OK.

Date: ________________

a) Microscope

Notes: ____

7. Dissolving PMMA

Dissolve the PMMA in acetone for 1 hour and subsequently emerge in ethanol and isopropyl alcohol (IPA) for 5 min.*

Date: ________________

*Let the sample dry at an angle

Samples	**Time in acetone (min)** *(60 min)*	**Time in ethanol (min)** *(5 min)*	**Time in IPA (min)** *(5 min)*

Notes: ____

8. Characterization

Do Raman spectroscopy for one sample on SiO_2 per foil.

Date: ________________

a) Microscope
b) Raman of SiO_2 sample.
Wavelength: _____ nm (*532 nm*) at _____ mW (*1 mW*). Si counts: ______ at ______ mW.

Notes: ____

Appendix I

Electrochemical measurement protocol

A series of electrochemical measurements are done to check the functioning of the system and to obtain data about the system in the form of IV-curves. Electrochemical measurements are done using the Bio-Logic SP300 potentiostat or the Bio-Logic VSP potentiostat in combination with EC-Lab software.

I.0.1 Calibration

Before, the IV-curves of the system are recorded, the electrodes are calibrated by placing the electrodes in the same reservoir. The open circuit voltage (OCV) is measured for 30 s to determine an offset between the electrodes. The OCV should be constant and smaller than 3 mV, otherwise the electrodes should be checked. Next, a chronopotentiometric (CP) measurement at $0.1, 1$ and 10 nA for 10 s each is done to check for an easy and stable current path.

I.0.2 Measurements

Subsequently, the electrodes are placed in different reservoirs. The WE is always placed at the graphene side of the device and the CE/RE is always placed at the SiN side. The following series of measurements method were used in the given order:

- Open circuit voltage (OCV)
- Chronoamperometry (CA)
- Cyclic voltammetry (CV)
- Potentio electrochemical impedance spectroscopy (PEIS)

The OCV is run for 10 s and CA measurement are run for 10 s at -1, 0 and 1 mV. These measurements are checked on irregularities before the CV measurement is continued. CVs will be run for 3 cycles at a scan rate of normally $10\,\mathrm{mVs^{-1}}$. The recorded signal is averaged over 5 measurements. At a regular scan from -1 to 1 V 16000 points are taken per cycle. The PEIS measurements are only conducted with the SP300 potentiostat. A scan is run from 1 MHz to 1 Hz with 10 points per decade. The signal has an amplitude of 10 mV and 2 measurements are averaged per frequency. After measurements both reservoirs are rinsed 3 times with DI water to remove all the salt from the device.

Appendix J

Materials

KCl is made with $\geq$ 99% potassium chloride of Sigma Aldrich dissolved in Milli-Q water.

Two different chip holders are used as is explained in section 3.2. For each chip holder a different set of reference electrodes is used. Robust saturated calomel electrode (SCE) (based on mercury and mercury(I)chloride) in saturated potassium chloride in water are used for the closed chip holder. These electrodes have a very low resistance and act as Faradiac contact.

For measurements with the open chip holder Ag/AgCl electrodes are synthesized using electro-deposition. Chloride was deposited on an silver wire with a diameter of 0.5 mm. The formed AgCl layer was grown for 1 hour at 21.15 µA in a solution of 0.1 M HCl and 1 M KCl. Before electro-deposition the wires were cleaned with fine sand paper and submerged in acetone for 20 min, whereafter the wires were rinsed with DI water.

Appendix K

IV-curves low voltage regime

CV measurements at low voltage are conducted on 5 chips. The CV measurements are run from -200 V to 200 V with a scan rate of $10\,\mathrm{mVs^{-1}}$. The devices are characterized in the closed device holder with SCEs connected to the Bio-Logic VSP potentiostat. 1 M KCl is used as electrolyte.

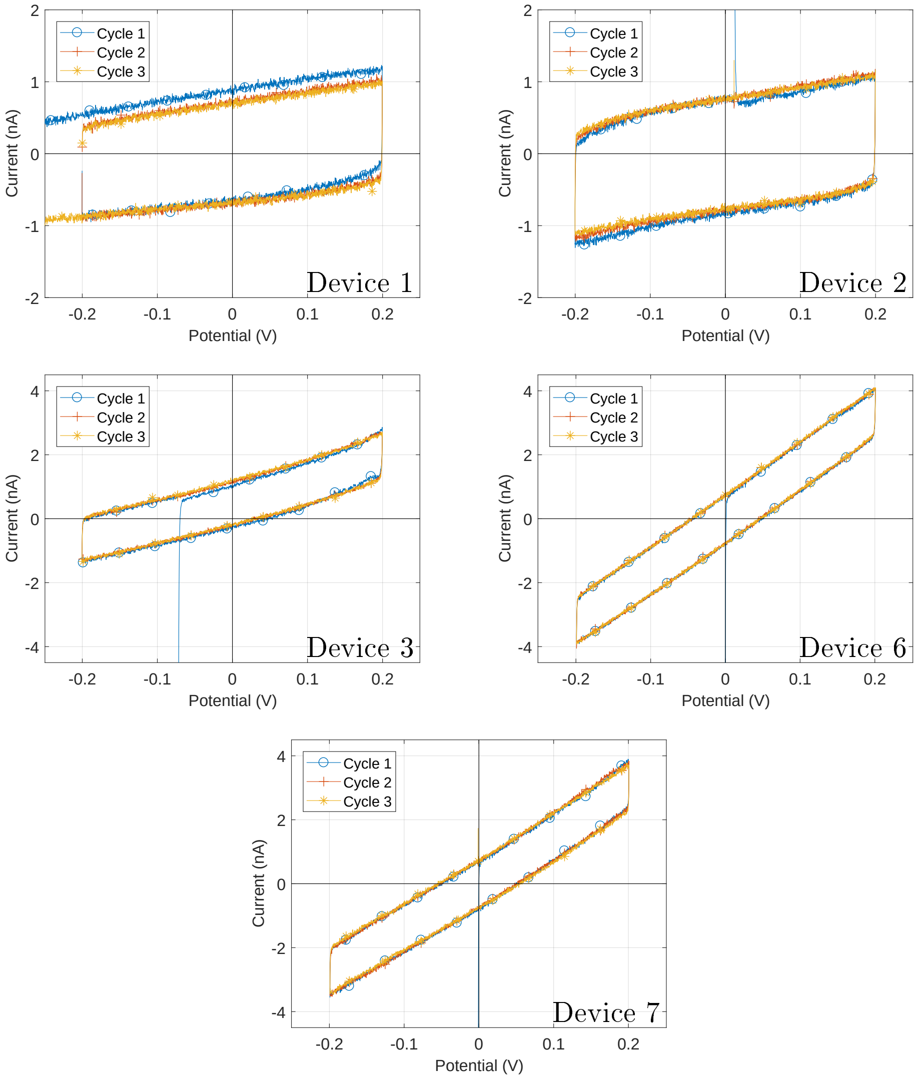

FIGURE K.1: CV measurements at low voltage in 1 M KCl for all graphene-SiN chips. The CV measurements are run from -200 mV to 200 mV with a scan rate of $10\,\mathrm{mVs^{-1}}$.

Appendix L

IV-curves low salt concentration

CV measurements at low voltage are conducted on 2 chips for different salt concentrations. 1 mM and 1 M KCl are used. The CV measurements are run from −200 V to 200 V with a scan rate of 10 mVs^{-1}. The devices are characterized in the closed device holder with SCEs connected to the Bio-Logic SP-300 potentiostat.

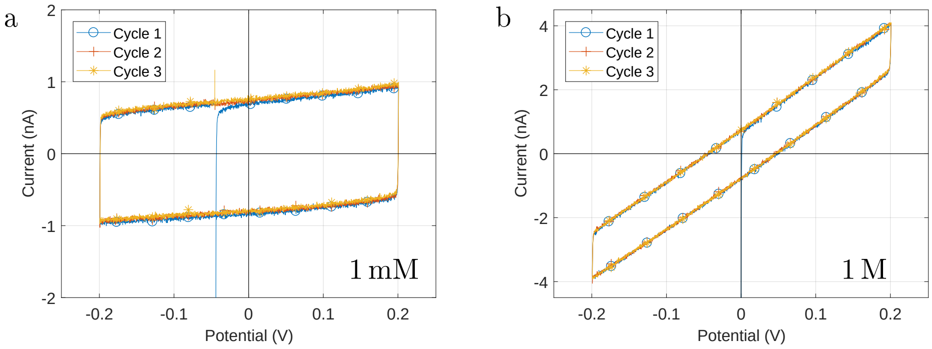

FIGURE L.1: IV-curves of device 6 for different salt concentrations. The voltage is swept between −200 V and 200 V with a scan rate of 10 mVs^{-10}.

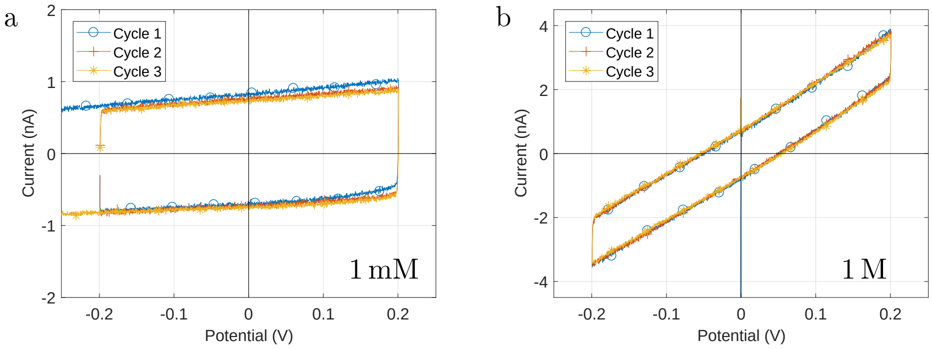

FIGURE L.2: IV-curves of Device 7 for different salt concentrations. The voltage is swept between −200 V and 200 V with a scan rate of 10 mVs^{-1}.

Appendix M

Proton transfer

Proton transfer as a real conductivity σ term for graphene: $\sigma = 3\,\mathrm{mScm}^{-2}$[47]. Conductivity of a 50 nm pore, due to proton transfer: $\pi r^2 \sigma = 6 \times 10^{-5}\,\mathrm{nS}$.

Assume detached graphene: Conductivity blister 2 µm, due to proton transfer: $\pi r^2 \sigma = 9 \times 10^{-2}\,\mathrm{nS}$.